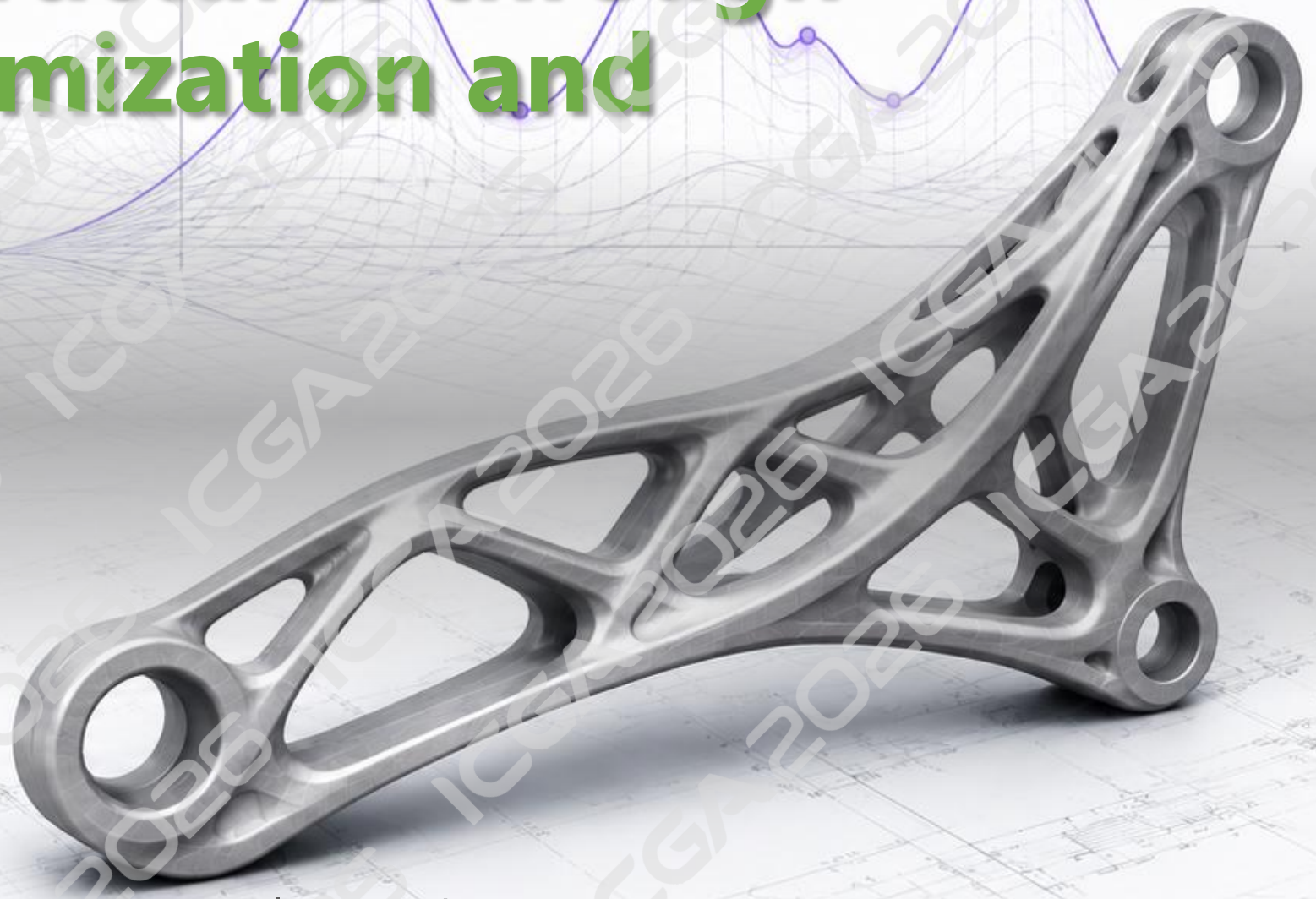
Computational Design of Sustainable Structures through Topology Optimization and Metamaterials



Junji Kato
Nagoya University

Nov. 2-4, 2026

ICGA2027, Xi'an International Conference Center | Xi'an, China

NAGOYA UNIVERSITY

Research Overview and Long-Term Vision

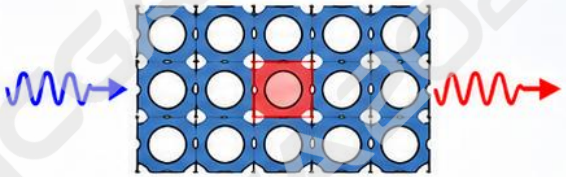
1. Research Overview and Long-Term Vision

Pillar 1: Nonlinear Multi-Material Topology Optimization



- Multi-material nonlinear topology optimization
- Subloading surface model for stable analysis
- Non-adjoint sensitivity (low cost)
- Stress-based interpolation (material-parameter free)

Pillar 2: Vibration/Wave Metamaterial Design

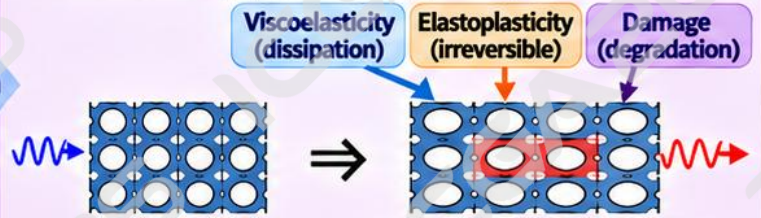


- Bandgap and defect-mode design (multiscale / supercell)
- One-way wave propagation (non-reciprocal design)

Integration

Long-Term Vision

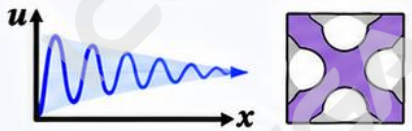
Computational design of nonlinear mechanical metamaterials with programmable wave propagation, tunable bandgaps, and energy dissipation.



2. Material Nonlinearity for Advanced Wave Control

Material nonlinearity enables new functionalities in vibration/wave metamaterials.

Viscoelasticity



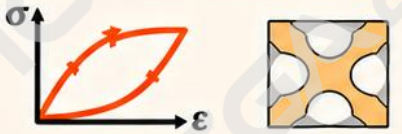
Frequency-selective damping

Hyperelasticity



Deformation-tunable bandgap

Elastoplasticity



Amplitude-dependent control

Damage mechanics



Damage-induced wave control (memory, reconfigurability)

Toward next-generation metamaterials by integrating material nonlinearity and wave control.

NAGOYA UNIVERSITY

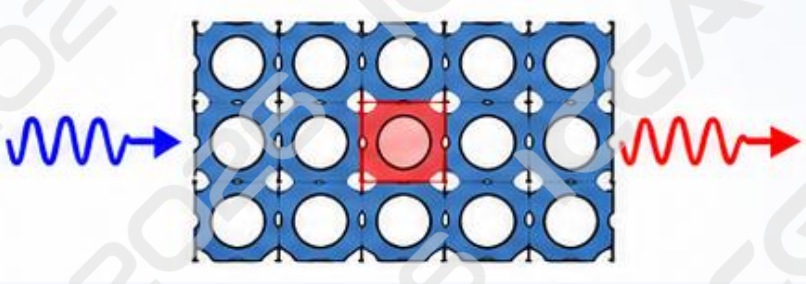
Contents

Pillar 1: Nonlinear Multi-Material Topology Optimization



- Composite of different constitutive laws
- Numerical instability -> Smooth function
- High computational cost
  -> Adjoint-free sensitivity (AFSA)
- Grayscale and complicated sensitivity
  -> Stress interpolation

Pillar 2: Vibration/Wave Metamaterial Design



- Bandgap and defect-mode design
- Multiscale / supercell approach
- Directional wave transmission

NAGOYA UNIVERSITY

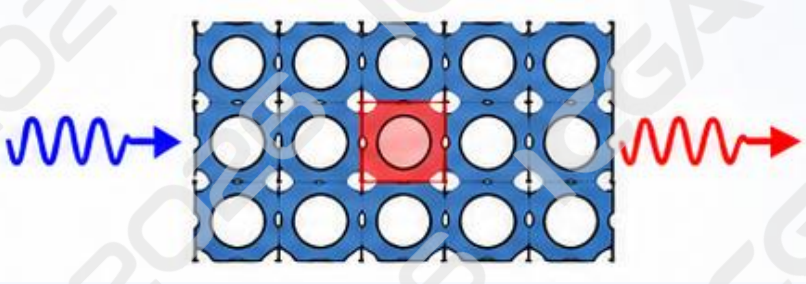
Contents

Pillar 1: Nonlinear Multi-Material Topology Optimization



- Composite of different constitutive laws
- Numerical instability -> Smooth function
- High computational cost
  -> Adjoint-free sensitivity (AFSA)
- Grayscale and complicated sensitivity
  -> Stress interpolation

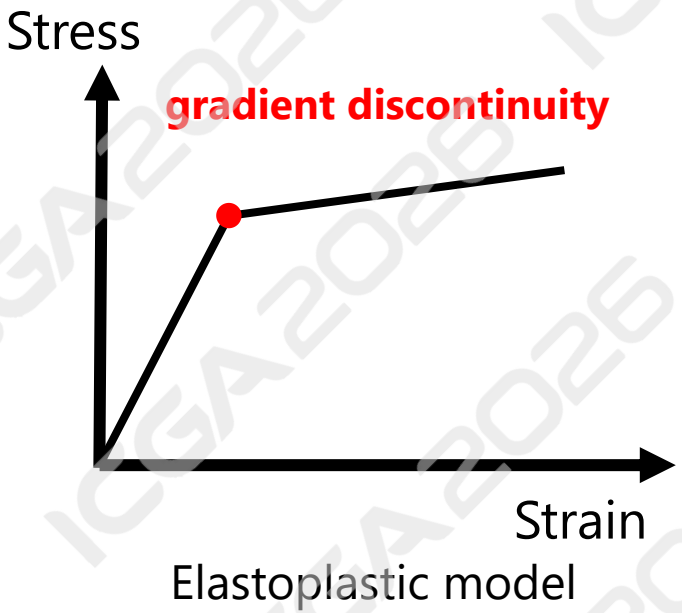
Pillar 2: Vibration/Wave Metamaterial Design



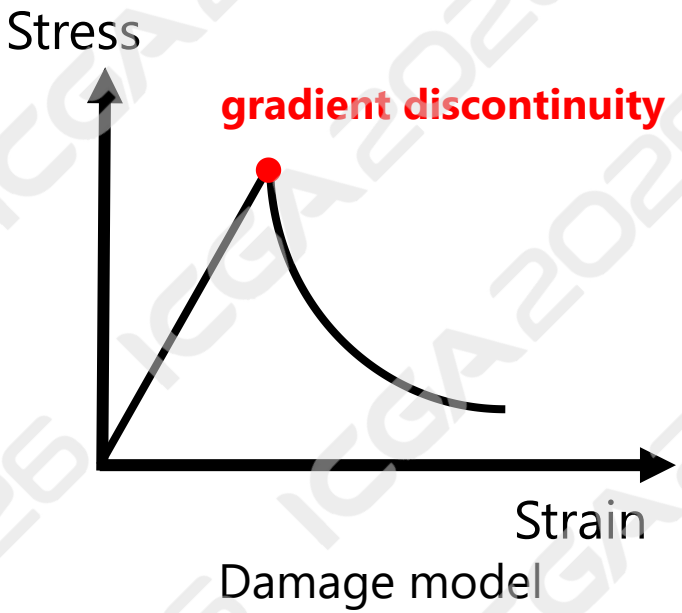
- Bandgap and defect-mode design
- Multiscale / supercell approach
- Directional wave transmission

Numerical instability in nonlinear multi-material TO

Difficulty in elastoplastic and damage models



Elastoplastic model



Damage model

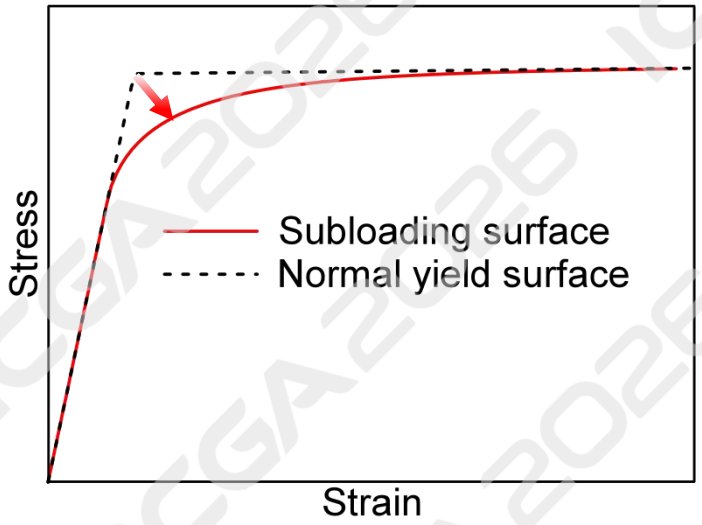


Optimization (ex. Damage model)

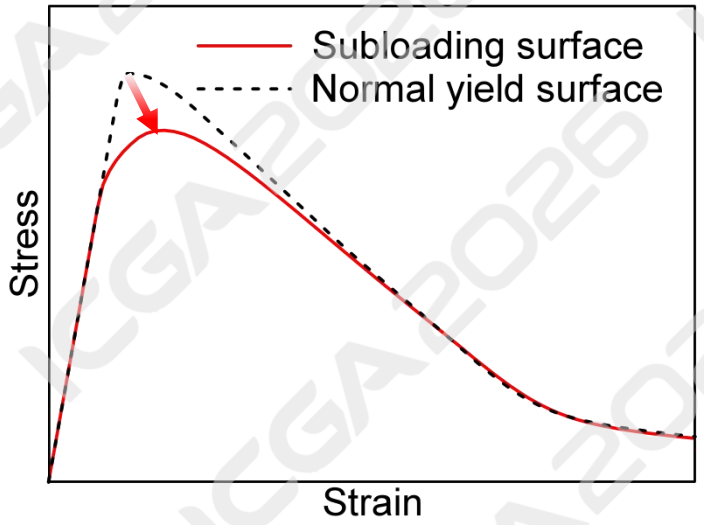
- Bad convergence due to material nonlinearity
- Gradient-based topology optimization requires the differentiability of the evaluated functions

Smoothed constitutive law | Subloading surface model

Smoothing stress-strain relationship



elastoplastic model



damage model

$$\Phi_{\mathrm{sub}}(\boldsymbol{\sigma}'^{\mathrm{eff}}, \bar{\varepsilon}^{\mathrm{p}}, R) = \|\boldsymbol{\sigma}'^{\mathrm{eff}}\| - \sqrt{\frac{2}{3}} R k(\bar{\varepsilon}^{\mathrm{p}}) \leq 0$$

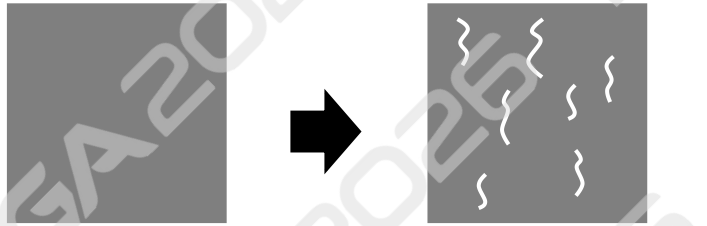
$$\begin{cases} \dot{R} = \|\dot{\boldsymbol{\varepsilon}}^{\mathrm{p}}\| U(R) = \dot{\gamma} U(R) \\ U(R) = u\left(\dfrac{1 - R_{\mathrm{e}}}{\langle R - R_{\mathrm{e}} \rangle} - 1\right) \end{cases}$$

- **Subloading surface model** (Hashiguchi, 1980) can eliminate gradient discontinuities
- Subloading surface model stabilizes TO process

Concept of elastoplastic-damage interpolation



elastoplastic body
(undamaged,
effective stress $\boldsymbol{\sigma}^{\mathrm{eff}}$)



elastoplastic body
(undamaged,
effective stress $\boldsymbol{\sigma}^{\mathrm{eff}}$)

elastoplastic body
(damaged,
nominal stress $\boldsymbol{\sigma}$)

$$\boldsymbol{\sigma} = (1 - D^{\mathrm{v}})\boldsymbol{\sigma}^{\mathrm{eff}}$$

effective stress $\boldsymbol{\sigma}^{\mathrm{eff}}$

effective stress $\boldsymbol{\sigma}^{\mathrm{eff}}$



nominal stress $\boldsymbol{\sigma}$

- TO based on material interpolation requires single constitutive model.
- Effective stress framework can express both ductile and quasi-brittle.
- Damage threshold κ^{th} is interpolated between materials.

ductile material
(large κ^{th})

quasi-brittle material
(small κ^{th})

Nara and Kato (2026), CMAME

NAGOYA UNIVERSITY

Damage model | some smoothing are utilized

① Equivalent strain (only tensile deformations contribute to damage evolution)

$$\tilde{\varepsilon} = \sqrt{\sum_{i=1}^{3} \langle \varepsilon_i \rangle^2}$$

② History variable κ progression

$$\kappa_{n+1} = \kappa_n + f_{\eta_s}(\tilde{\varepsilon}_{n+1} - \kappa_n)$$

$$f_\eta(\tilde{\varepsilon} - \kappa_n) = \begin{cases} 0 & (\tilde{\varepsilon} - \kappa_n \le 0) \\ \dfrac{(\tilde{\varepsilon} - \kappa_n)^2}{2\eta} & (0 < \tilde{\varepsilon} - \kappa_n \le \eta) \\ (\tilde{\varepsilon} - \kappa_n) - \dfrac{\eta}{2} & (\eta < \tilde{\varepsilon} - \kappa_n) \end{cases}$$

non-smooth

⚠ $\kappa_{n+1} = \max(\kappa_n, \tilde{\varepsilon}_{n+1})$

③ Judgement of damage occurrence

$$\kappa^{\mathrm{act}} = \frac{\kappa + \kappa^{\mathrm{th}} + \sqrt{(\kappa - \kappa^{\mathrm{th}})^2 + \epsilon}}{2}$$

non-smooth

⚠ $\kappa^{\mathrm{act}}_{n+1} = \max(\kappa_{n+1}, \kappa^{\mathrm{th}})$

④ Calculation of damage variable (Mazars and Pyaudier-Cabot (1989))

$$D = 1 - \left[\frac{\kappa^{\mathrm{th}}(1-a)}{\kappa^{\mathrm{act}}} + \frac{a}{\exp b(\kappa^{\mathrm{act}} - \kappa^{\mathrm{th}})} \right]$$

⑤ Viscous regularization (Duvaut and Lions (1976))

$$D^{\mathrm{v}}_{n+1} = \frac{\tau}{\tau + \Delta t} D^{\mathrm{v}}_n + \frac{\Delta t}{\tau + \Delta t} D_{n+1}$$

Nara and Kato (2026), CMAME

Optimization problem

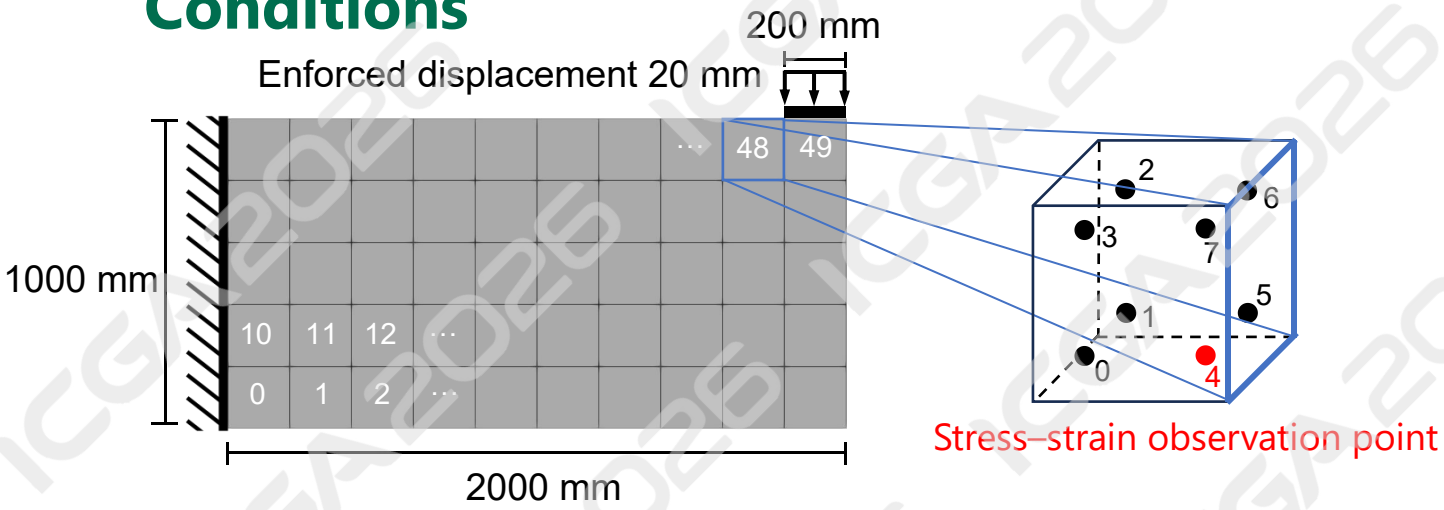
Optimization problem

Objective function	minimize	$f(\boldsymbol{s}) = -\int_{\Omega}\int_{\hat{\varepsilon}} \boldsymbol{\sigma} : \mathrm{d}\boldsymbol{\varepsilon}\,\mathrm{d}\Omega$	Maximizing energy absorption capacity
Constraint	subject to	$g(\boldsymbol{s}) = \int_{\Omega} s_j\,\mathrm{d}\Omega - \hat{V} \leq 0$	Volume of ductile material
Design variable	$s_j = \dfrac{r_j}{r_0}$	$0 \leq s_j \leq 1$	Material volume fraction

- Material parameters interpolation based on SIMP method
- Derived sensitivity based on path-dependent adjoint variable method (Alberdi et al., 2018)
- MMA

Numerical example | Sensitivity verification

Conditions



displacement incremental: 0.4 mm,

Poisson ratio $\nu = 0.3$

$R_e = 0.7$, $u_0 = 150$, $\alpha = 100$, $\beta = 0.02$

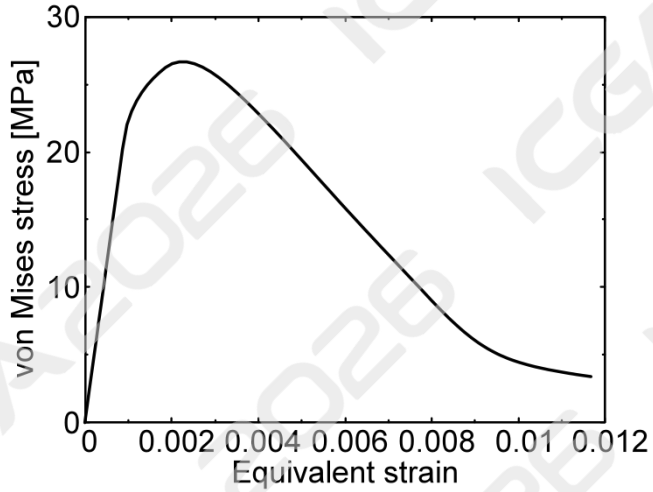
$a = 0.9$, $b = 500$

	Quasi-brittle	Ductile
Elastic modulus E [MPa]	30,000	210,000
Initial yield stress σ_Y [MPa]	30.0	300
Elastoplastic tangent modulus E^{ep} [MPa]	10.0	500
Damage threshold κ^{th}	0.001	0.2

- Comparison of analytical sensitivity with FDA
- Conducted with three initial design variables (s_0 = 0.1, 0.5, 0.9)

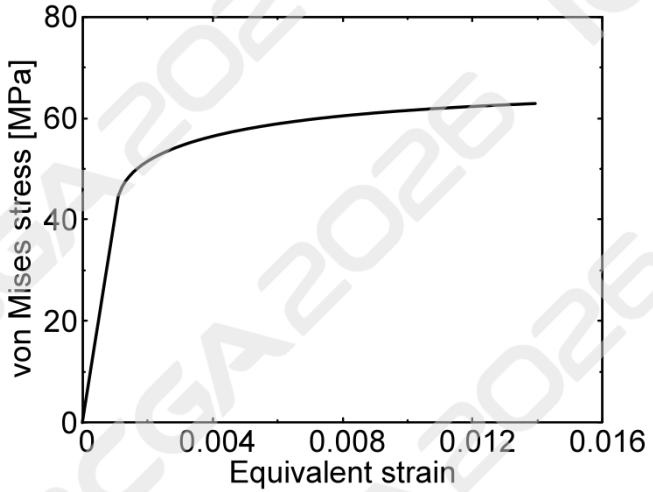
Numerical example | Sensitivity verification

Nara and Kato (2026), CMAME



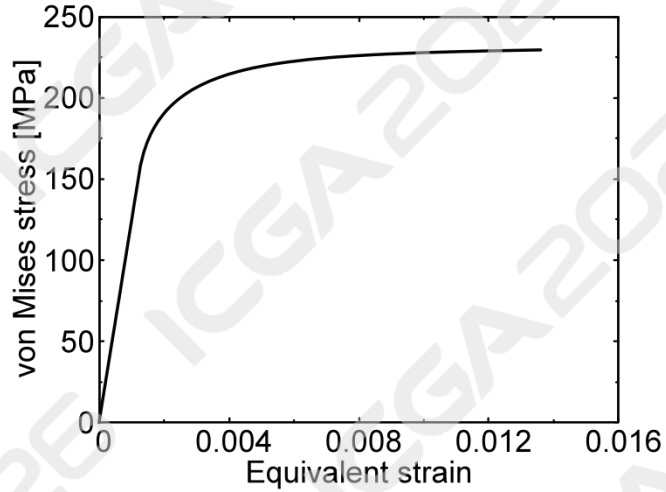
s_0 = 0.1

almost **quasi-brittle**



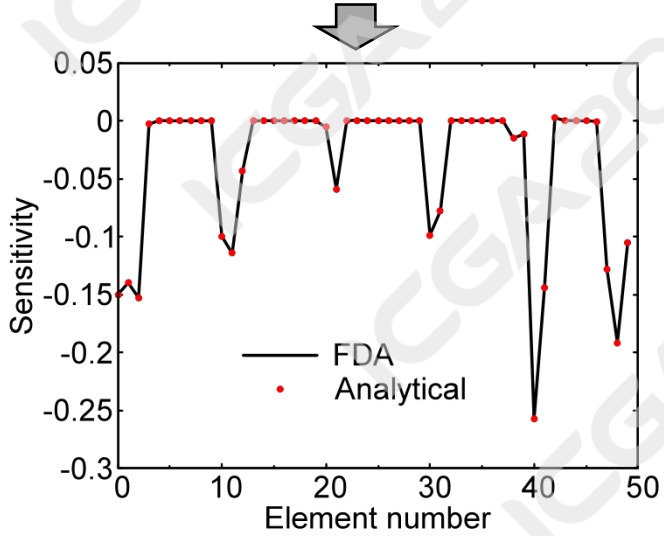
s_0 = 0.5

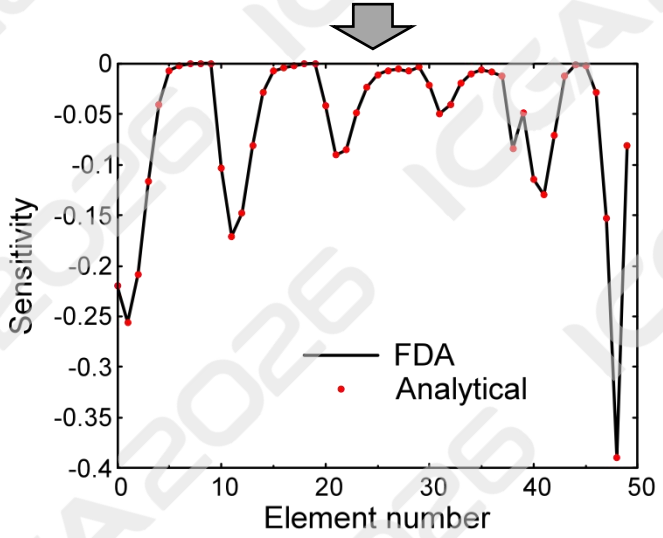
intermediate

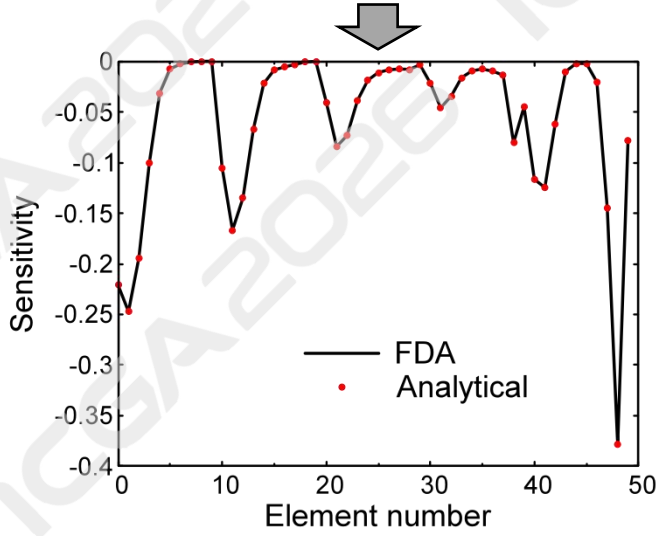


s_0 = 0.9

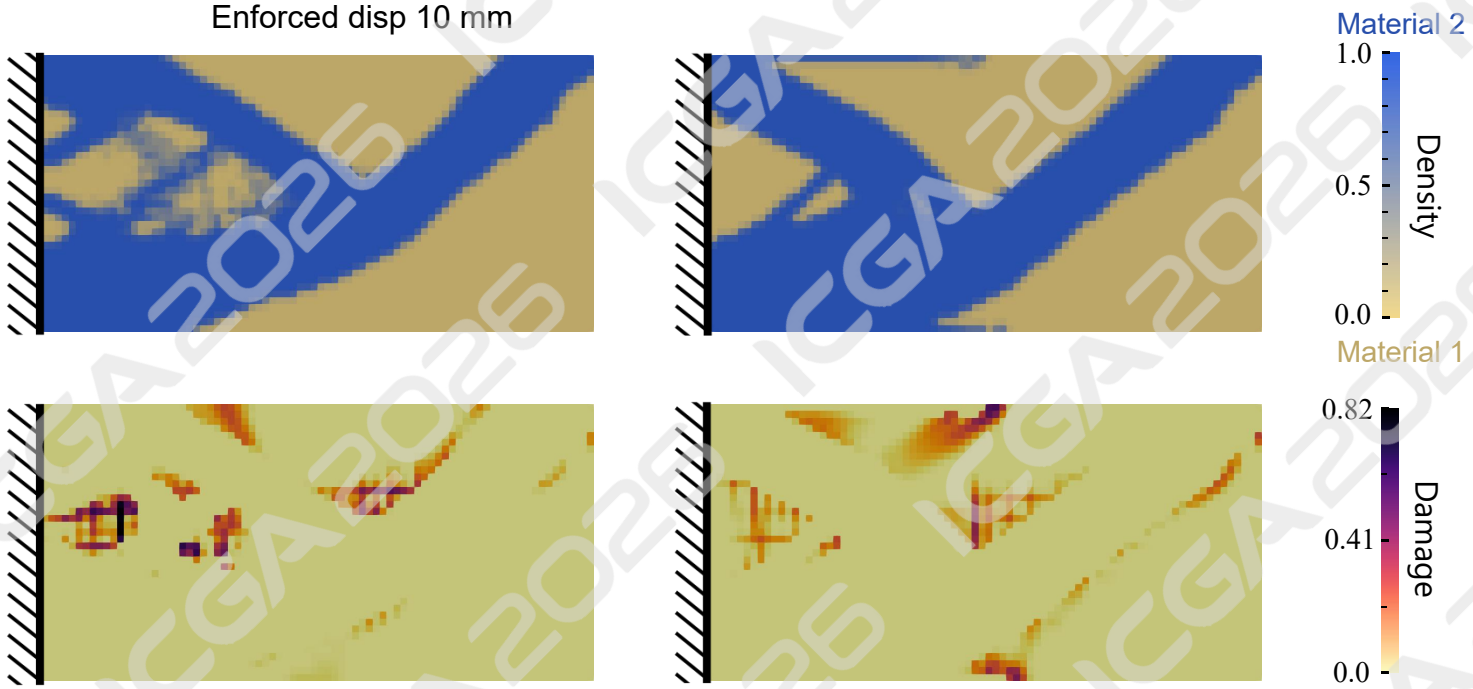
almost **ductile**







Numerical example | Optimization result 1



M_{nd}: 12.16 %

$f = -7.17 \times 10^6$

Conventional method (without smoothing)

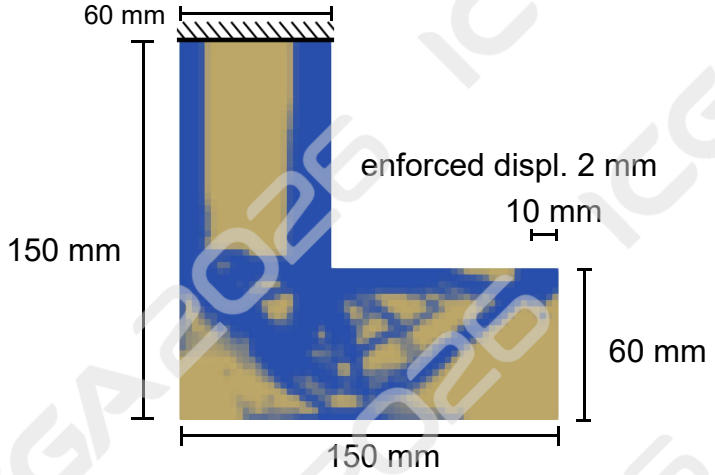
M_{nd}: 7.11 %

$f = -7.47 \times 10^6$

Proposed method (with smoothing)

- Proposed method improved convergence
- Proposed method enhanced ductility of structure

Numerical example | Optimization result

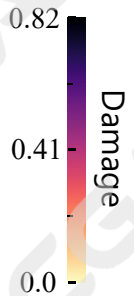












M_{nd}: 20.41 %

$f = -6.03 \times 10^6$

Conventional method (without smoothing)

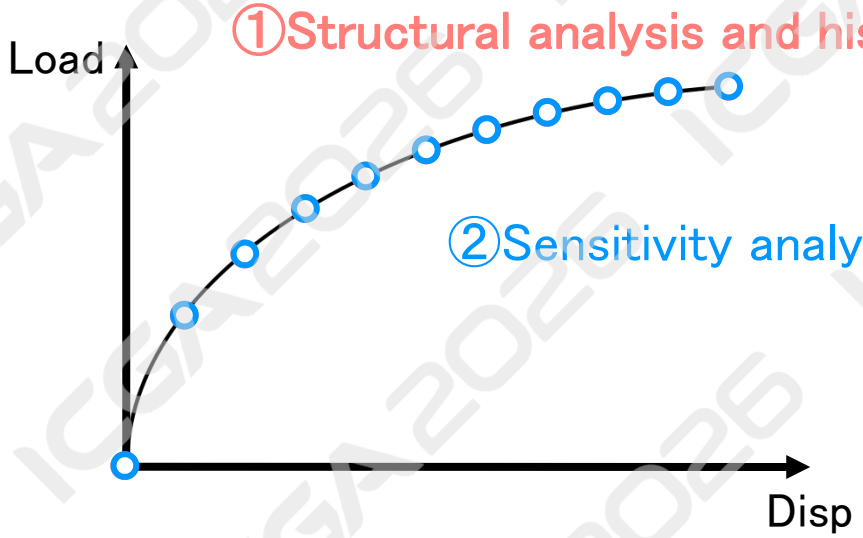
M_{nd}: 13.56 %

$f = -6.54 \times 10^6$

Proposed method (with smoothing)

High computational cost in adjoint variable sensitivity

Path-dependent adjoint variable method



$$f(\boldsymbol{s}) = F(\boldsymbol{s}, \boldsymbol{u}_1, \ldots, \boldsymbol{u}_{n_{\text{step}}}, \boldsymbol{c}_1, \ldots, \boldsymbol{c}_{n_{\text{step}}})$$

$$\hat{f} = f(\boldsymbol{s}) + \sum_{n=1}^{n_{\text{step}}} \boldsymbol{\lambda}_n^{\mathrm{T}} \boldsymbol{R}_n + \sum_{n=1}^{n_{\text{step}}} \boldsymbol{\mu}_n^{\mathrm{T}} \boldsymbol{H}_n$$

$$\begin{cases} \dfrac{\partial F}{\partial \boldsymbol{u}_n} + \boldsymbol{\lambda}_{n+1}^{\mathrm{T}} \dfrac{\partial \boldsymbol{R}_{n+1}}{\partial \boldsymbol{u}_n} + \boldsymbol{\mu}_{n+1}^{\mathrm{T}} \dfrac{\partial \boldsymbol{H}_{n+1}}{\partial \boldsymbol{u}_n} + \boldsymbol{\lambda}_n^{\mathrm{T}} \dfrac{\partial \boldsymbol{R}_n}{\partial \boldsymbol{u}_n} + \boldsymbol{\mu}_n^{\mathrm{T}} \dfrac{\partial \boldsymbol{H}_n}{\partial \boldsymbol{u}_n} = \boldsymbol{0} \\ \dfrac{\partial F}{\partial \boldsymbol{c}_n} + \boldsymbol{\lambda}_{n+1}^{\mathrm{T}} \dfrac{\partial \boldsymbol{R}_{n+1}}{\partial \boldsymbol{c}_n} + \boldsymbol{\mu}_{n+1}^{\mathrm{T}} \dfrac{\partial \boldsymbol{H}_{n+1}}{\partial \boldsymbol{c}_n} + \boldsymbol{\lambda}_n^{\mathrm{T}} \dfrac{\partial \boldsymbol{R}_n}{\partial \boldsymbol{c}_n} + \boldsymbol{\mu}_n^{\mathrm{T}} \dfrac{\partial \boldsymbol{H}_n}{\partial \boldsymbol{c}_n} = \boldsymbol{0} \end{cases}$$

Global adjoint equation

- High sensitivity accuracy
- Huge computational time and memory consumption
- Complicated formulation

Adjoint-free-sensitivity analysis (AFSA)

Adjoint-free sensitivity analysis[1] and its challenges

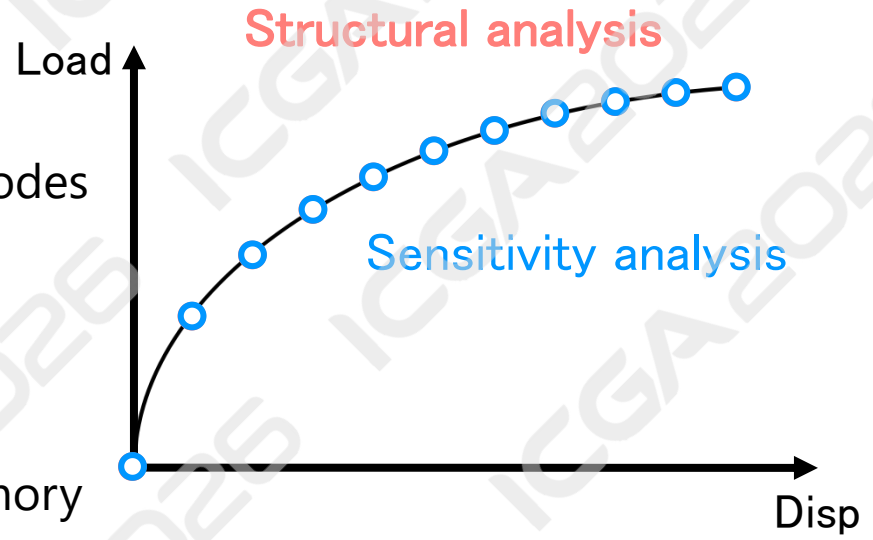
Kato (2015A), SMO

What is Adjoint-free sensitivity analysis (AFSA)?



Load works only displacement control nodes

- Forward and local sensitivity calculation
- Expectation of high speed and low memory



Remaining challenges and research subjects

- Lack of quantitative evaluation of computational cost
- Difficulties in modifying or extending material models due to the complexity of sensitivity formulation
  (Obtaining the required stress sensitivity $\nabla^*_{s_j}\boldsymbol{\sigma}_n$ requires differentiating the entire constitutive model)

Analysis method

Sensitivity derivation based on Kato et al. (2015a)

- Objective function

$$\text{minimize} \quad f(\boldsymbol{s}) = -\int_{\Omega}\int_{\hat{\varepsilon}} \boldsymbol{\sigma} : \mathrm{d}\boldsymbol{\varepsilon}\,\mathrm{d}\Omega$$

- Direct differentiation of discretized objective function at load step n+1

$$\nabla_{s_j} f(\boldsymbol{s}) = -\int_{\Omega}\int_{0}^{t} \left[\nabla^*_{s_j}\boldsymbol{\sigma} : \dot{\boldsymbol{\varepsilon}} + \underline{\left(\mathbb{C} : \nabla_{s_j}\boldsymbol{\varepsilon}\right) : \dot{\boldsymbol{\varepsilon}} + \boldsymbol{\sigma} : \nabla_{s_j}\dot{\boldsymbol{\varepsilon}}}\right] \mathrm{d}t\,\mathrm{d}\Omega$$

Implicit terms

- Load works only displacement control nodes
- Symmetric tangent stiffness tensor

- Sensitivity of discretized objective function at load step n+1

$$\nabla_{s_j} f_{n+1}(\boldsymbol{s}) = -\int_{\Omega} \underline{\nabla^*_{s_j}\boldsymbol{\sigma}_{n+1}} : \Delta\boldsymbol{\varepsilon}_{n+1}\,\mathrm{d}\Omega$$

Explicit term

$\nabla^*_{s_j}$ is current strain-fixed derivative

Stress interpolation

Stress interpolation

Stress interpolation[2, 3, 4]

$$\boldsymbol{\sigma}_n = (1 - s_j^p)\boldsymbol{\sigma}_n^{(1)} + s_j^p \boldsymbol{\sigma}_n^{(2)}$$

- Elimination of design-dependent material parameters
- Arbitrary constitutive laws for each phase

Conditional stress sensitivity

$$\nabla_{s_j}^* \boldsymbol{\sigma}_n = p s_j^{p-1} \left(\boldsymbol{\sigma}_n^{(2)} - \boldsymbol{\sigma}_n^{(1)} \right) + (1 - s_j^p) \nabla_{s_j}^* \boldsymbol{\sigma}_n^{(1)} + s_j^p \nabla_{s_j}^* \boldsymbol{\sigma}_n^{(2)}$$

Following Kato et al. (2015), the stress sensitivity in each phase vanishes

- Only stress is required to obtain sensitivity
- Reformulation is completely unnecessary when changing models

[2] Kato et al. (2015b), IJNME
[3] Han et al. (2026), CMAME
[4] Nara and Kato (2026), CMAME, prepared

NAGOYA UNIVERSITY

Analysis method

離散化→微分から
微分→離散化に変更

Objective function sensitivity

$$\nabla_{s_j} f(\boldsymbol{s}) = -\int_\Omega \int_0^t \left[\nabla^*_{s_j} \boldsymbol{\sigma} : \dot{\boldsymbol{\varepsilon}} + \cancel{\left(\mathbb{C} : \nabla_{s_j} \boldsymbol{\varepsilon}\right) : \dot{\boldsymbol{\varepsilon}} + \boldsymbol{\sigma} : \nabla_{s_j} \dot{\boldsymbol{\varepsilon}}} \right] \mathrm{d}t \, \mathrm{d}\Omega$$

Start from principle of virtual work

$$\int_\Omega \boldsymbol{\sigma} : \nabla_{s_j} \boldsymbol{\varepsilon} \, \mathrm{d}\Omega - \lambda \cancel{\int_\Gamma \boldsymbol{t}_0 \cdot \nabla_{s_j} \boldsymbol{u} \, \mathrm{d}\Gamma} = 0$$

Load works only at displacement control nodes

$$\int_\Omega \left[\dot{\boldsymbol{\sigma}} : \nabla_{s_j} \boldsymbol{\varepsilon} + \boldsymbol{\sigma} : \nabla_{s_j} \dot{\boldsymbol{\varepsilon}} \right] \mathrm{d}\Omega = 0$$

Time derivation

$$\int_\Omega \left[\left(\mathbb{C} : \nabla_{s_j} \boldsymbol{\varepsilon}\right) : \dot{\boldsymbol{\varepsilon}} + \boldsymbol{\sigma} : \nabla_{s_j} \dot{\boldsymbol{\varepsilon}} \right] \mathrm{d}\Omega = 0$$

Utilizing

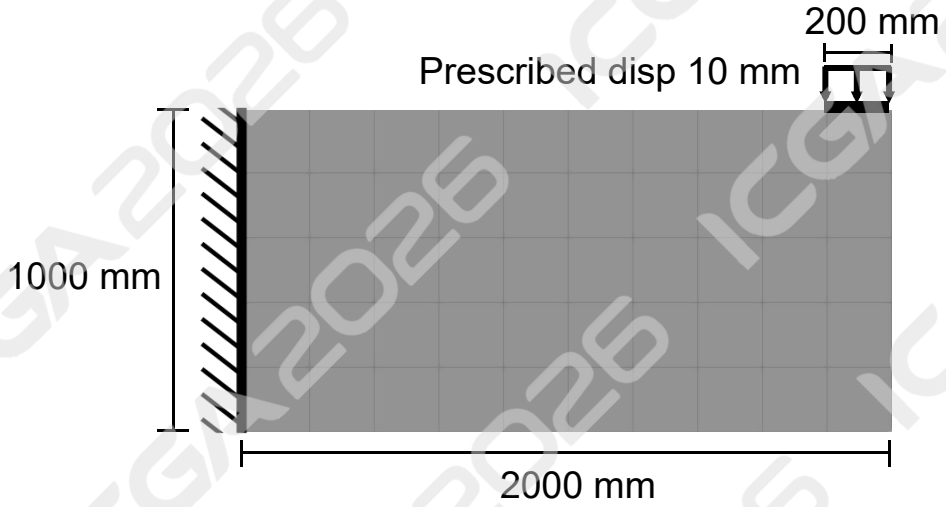
$$\dot{\boldsymbol{\sigma}} = \mathbb{C} : \dot{\boldsymbol{\varepsilon}}$$

$$\dot{\boldsymbol{\sigma}} : \nabla_{s_j} \boldsymbol{\varepsilon} = \left(\mathbb{C} : \nabla_{s_j} \boldsymbol{\varepsilon}\right) : \dot{\boldsymbol{\varepsilon}}$$

Assuming tangent stiffness $\mathbb{C}$ is symmetric

Numerical example | computational cost

Conditions of evaluation



[4]

	Material 1	Material 2
Elastic modulus E [MPa]	30,000	210,000
Initial yield stress σ_Y [MPa]	30.0	300
Elastoplastic tangent modulus E^{ep} [MPa]	10.0	500

Load step: 50 (displacement incremental is 0.2 mm)

Yield criteria: von Mises

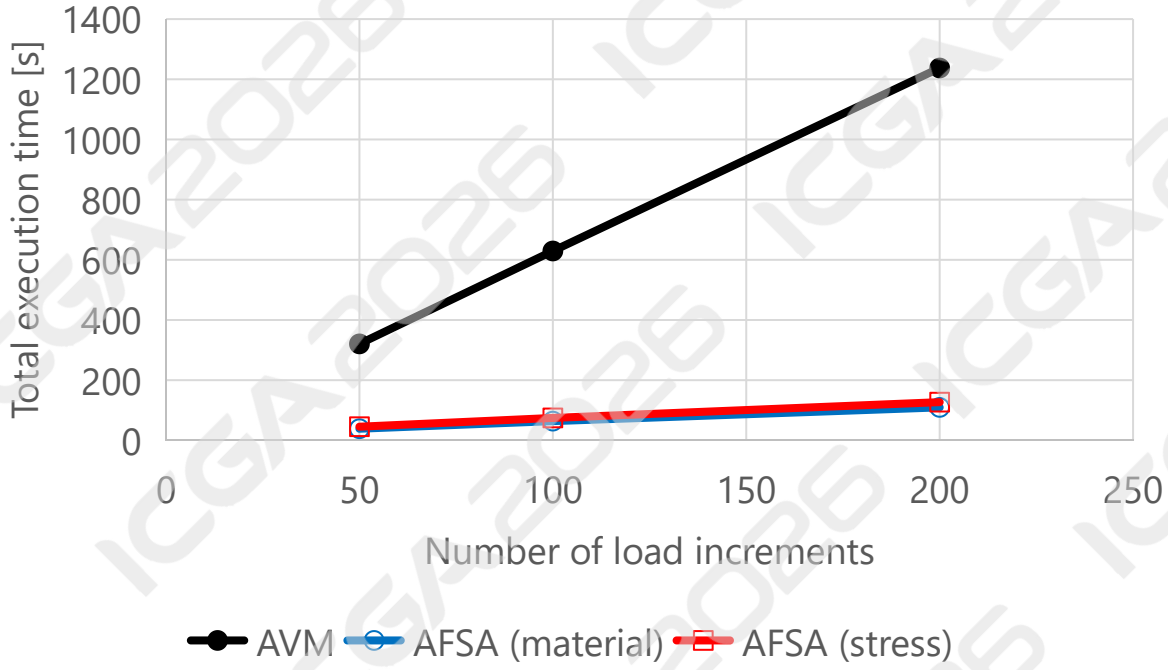
Hardening: isotropic linear

- Confirming conditions before comparing computational cost
- Three types of sensitivities match

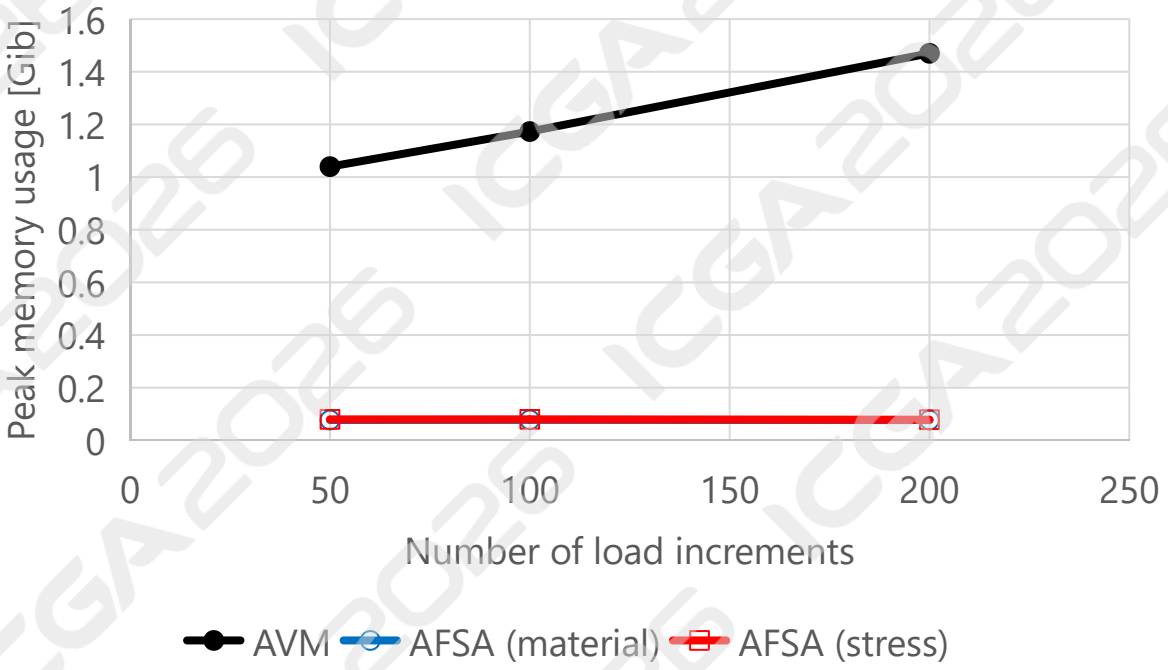
[4] Nara and Kato (In preparation)

Numerical example | computational cost

Results of evaluation



(a) Total execution time (Wall-clock time)



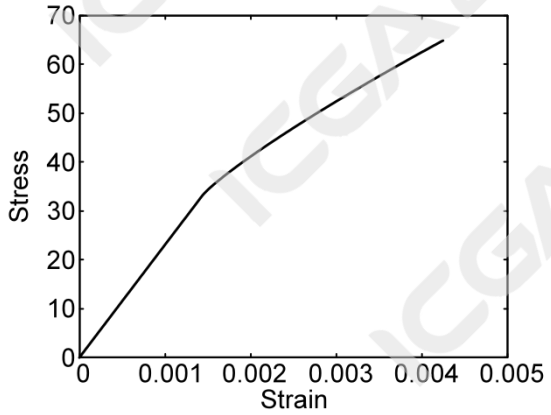
(b) Peak memory usage

CPU: 2 × Intel Xeon Gold 6326 (2.90GHz, 16 cores each)
Parallelization: OpenMP, 8 threads (pinned to CPU cores 0-7)
Implementation: Eigen, compiler optimization -03
Optimization: 3 optimization steps
Measurement: 10 runs per condition

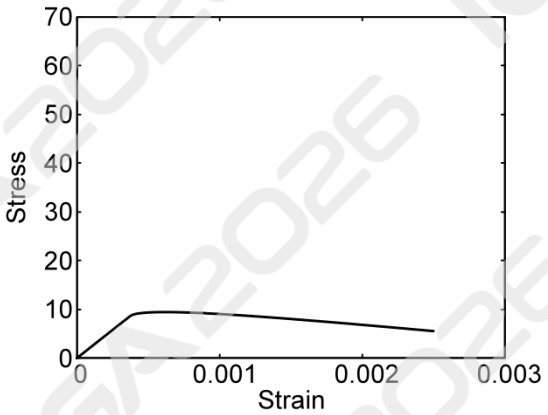
Numerical example | Multi-material TO

Constitutive law

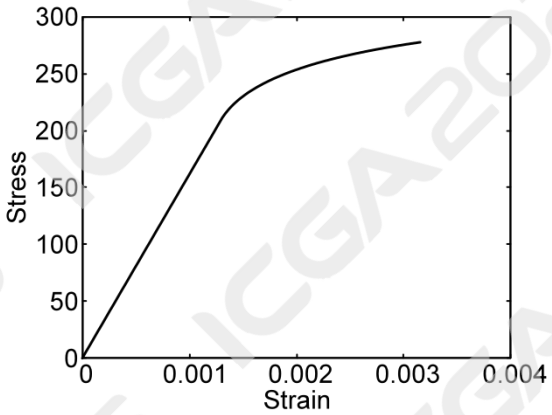
	Material 1 (Drucker-Prager)	Material 2 (von Mises)
Yield function	$\Phi_{\mathrm{sub}} = \|\boldsymbol{\sigma}'\| + \sqrt{2}\eta p - \sqrt{2}\xi Rk(\bar{\varepsilon}^{\mathrm{p}}) \leq 0$	$\Phi_{\mathrm{sub}} = \|\boldsymbol{\sigma}'\| - \sqrt{\frac{2}{3}} Rk(\bar{\varepsilon}^{\mathrm{p}}) \leq 0$
Flow rule	$\dot{\boldsymbol{\varepsilon}}^{\mathrm{p}} = \dot{\gamma}\frac{\partial \Phi_{\mathrm{sub}}}{\partial \boldsymbol{\sigma}} = \dot{\gamma}\frac{\boldsymbol{\sigma}'}{\|\boldsymbol{\sigma}'\|}$	$\dot{\boldsymbol{\varepsilon}}^{\mathrm{p}} = \dot{\gamma}\frac{\partial \Phi_{\mathrm{sub}}}{\partial \boldsymbol{\sigma}} = \dot{\gamma}\frac{\boldsymbol{\sigma}'}{\|\boldsymbol{\sigma}'\|}$
Equivalent plastic strain evolution	$\dot{\bar{\varepsilon}}^{\mathrm{p}} = \sqrt{2}\xi\dot{\gamma}$	$\dot{\bar{\varepsilon}}^{\mathrm{p}} = \sqrt{\frac{2}{3}}\dot{\gamma}$



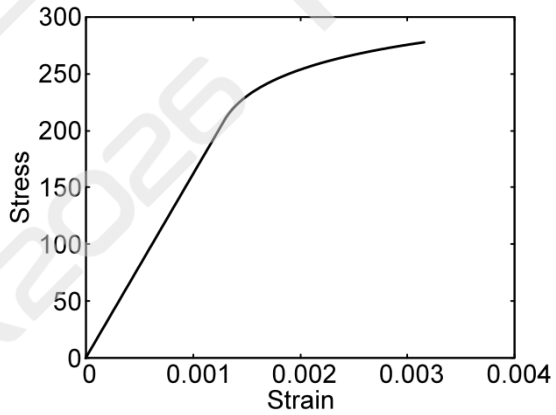
Compression (Material 1)



Tension (Material 1)



Compression (Material 2)

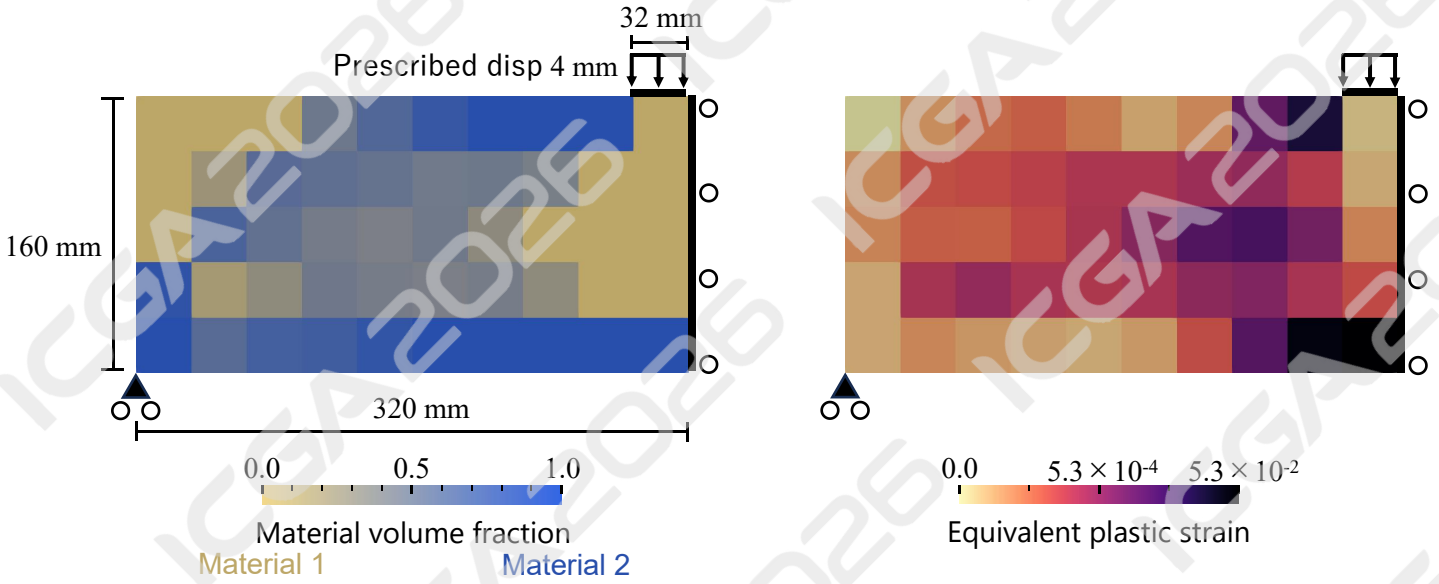


Tension (Material 2)

Numerical example｜Multi-material TO

感度の精度検証を非一様のトポロジーで実施

Sensitivity verification



	Material 1 (Drucker-Prager)	Material 2 (von Mises)
Elastic modulus E [MPa]	30,000	210,000
Initial yield stress σ_Y [MPa]	30.0	300
Elastoplastic tangent modulus E^{ep} [MPa]	10.0	500

L2-norm error: 0.732%

Displacement incremental: 0.04 mm,

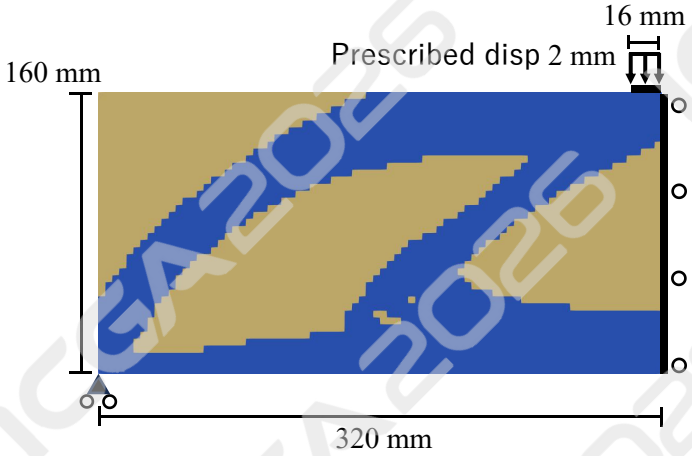
Poisson ratio $\nu = 0.3$,

SIMP penalty $p = 3$,

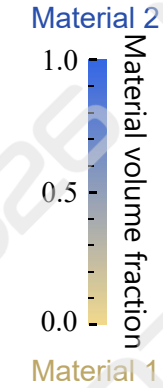
$\eta = 0.5$ (Drucker-Prager)

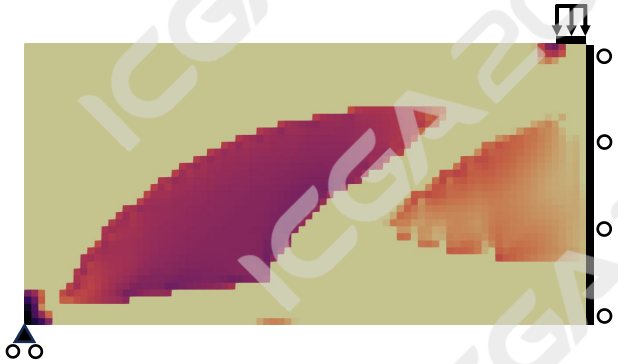
Numerical example | Multi-material TO

Optimization results

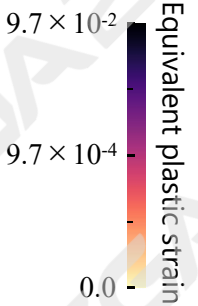












$f = -1.34 \times 10^4$

mat1: von Mises
mat2: von Mises

$f = -1.46 \times 10^4$

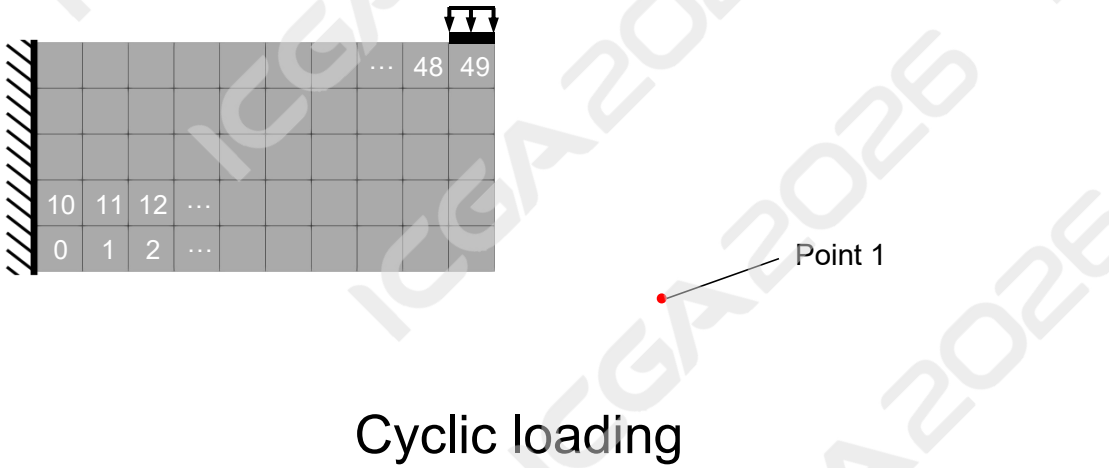
mat1: Drucker-Prager
mat2: von Mises

8.96% increase in energy absorption through pressure-dependent modeling

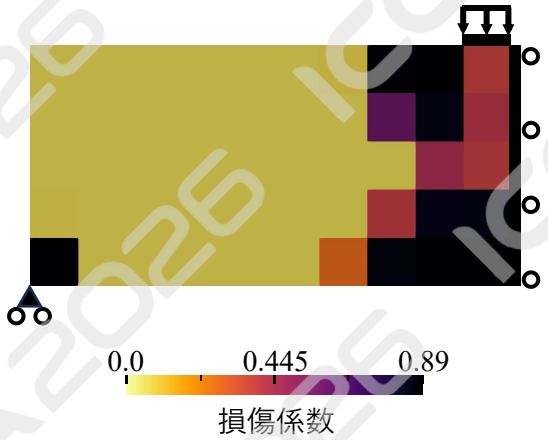
Numerical example｜Limitation

感度不一致のグラフ差し替え，その他の限界の追加

Conditions of inapplicability



Cyclic loading



Damage model (Simo and Ju, 1987)

Other limitations

- Symmetric tangent stiffness
- Only displacement control
- Ignoring body forces
- Small deformation assumption
- Limited to external work maximization

NAGOYA UNIVERSITY

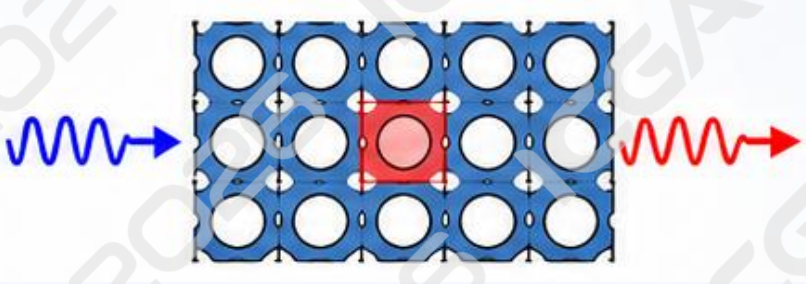
Contents

Pillar 1: Nonlinear Multi-Material Topology Optimization



- Composite of different constitutive laws
- Numerical instability -> Smooth function
- High computational cost
  -> Adjoint-free sensitivity (AFSA)
- Grayscale and complicated sensitivity
  -> Stress interpolation

Pillar 2: Vibration/Wave Metamaterial Design



- Bandgap and defect-mode design
- Multiscale / supercell approach
- Directional wave transmission

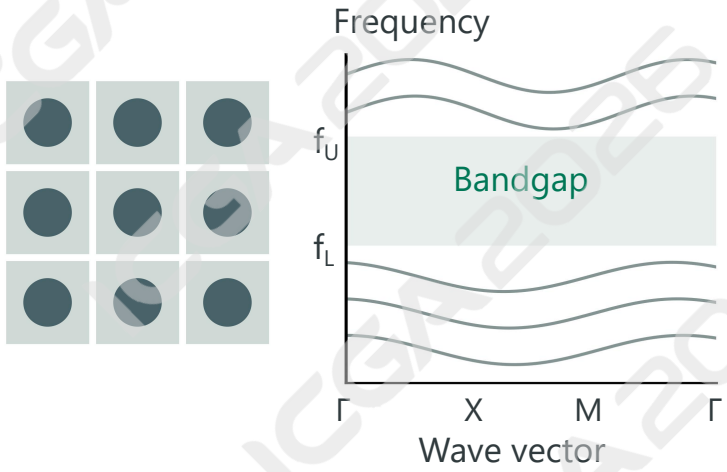
Localized Vibrations in Phononic Crystals

Background: Phononic bandgaps suppress propagating elastic waves.

Motivation: Prescribed local resonances concentrate vibration at selected sites for frequency-selective sensing and energy concentration.

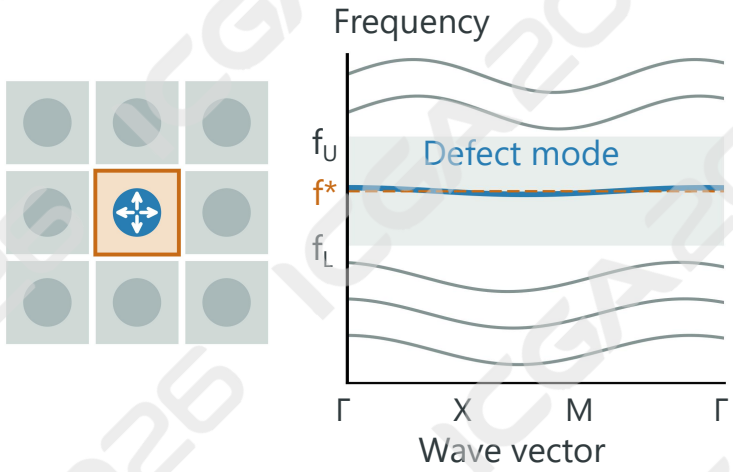
Challenge: place a localized resonance at a chosen frequency while separating competing modes.

Stage I: host bandgap



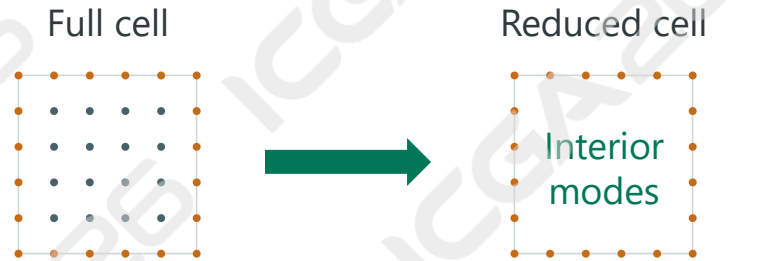
Host-cell optimization opens a bandgap.

Stage II: localized mode



Supercell defect optimization creates an in-gap localized mode.

CB acceleration



Interface DOFs retained

Repeated analyses are costly.
Reduce the cell interior and reuse the fixed host matrices.

Goal: localize vibration within a defect near a prescribed target frequency.

Xinlin Xu, Junji Kato, Reduced-order topology optimization of defect spectra in phononic crystals, 2026, CMAME, submitted and (arXiv:2605.26435)
Xinlin Xu, Junji Kato, Topology optimization for multiple prescribed defect resonances in phononic crystals, 2026, JSV, submitted

NAGOYA UNIVERSITY

Problem Formulation

One target frequency

P_a attracts modes toward the target.
P_r pushes competing modes toward gap edges.

$$\min_{\boldsymbol{s}} \; J_{\text{single}} = \underbrace{\sum_{j\in\mathcal{D}} S_j P_a(f_j)}_{\text{Attraction}} + \underbrace{w_r \sum_{j\in\mathcal{D}} (1-S_j) P_r(f_j)}_{\text{Repulsion}}$$

attract the target frequency move competing modes outward

$$\text{subject to} \quad \frac{V(\boldsymbol{s})}{V_{\text{D}}} \le \overline{V}.$$

$$P_{\text{a}}(f_j) = \left(\frac{f_j - f^{\star}_{\text{def}}}{f^{\star}_{\text{def}}}\right)^2, \quad P_{\text{r}}(f_j) = \exp\left[-\frac{(f_j - f_{\text{M}})^2}{2\sigma_{\text{r}}^2}\right],$$

$$S_j = \exp\left[-\left(\frac{f_j - f^{\star}_{\text{def}}}{\sigma_{\text{s}}}\right)^{2\beta_{\text{s}}}\right], \quad f_{\text{M}} = \frac{f_{\text{L}} + f_{\text{U}}}{2}.$$

S_j selects modes by distance to the target;
several modes nearby can be attracted.

NAGOYA UNIVERSITY

Problem Formulation

One target frequency

P_a attracts modes toward the target.
P_r pushes competing modes toward gap edges.

$$\min_{\boldsymbol{s}} \; J_{\text{single}} = \sum_{j \in \mathcal{D}} \left[S_j P_a(f_j) + w_r (1 - S_j) P_r(f_j) \right]$$

$$\text{subject to} \quad \frac{V(\boldsymbol{s})}{V_D} \le \overline{V}.$$

$$P_a(f_j) = \left(\frac{f_j - f^\star_{\text{def}}}{f^\star_{\text{def}}} \right)^2, \quad P_r(f_j) = \exp\left[-\frac{(f_j - f_M)^2}{2\sigma_r^2} \right],$$

$$S_j = \exp\left[-\left(\frac{f_j - f^\star_{\text{def}}}{\sigma_s} \right)^{2\beta_s} \right], \quad f_M = \frac{f_L + f_U}{2}.$$

S_j selects modes by distance to the target; several nearby modes can be attracted.

Multiple target frequencies

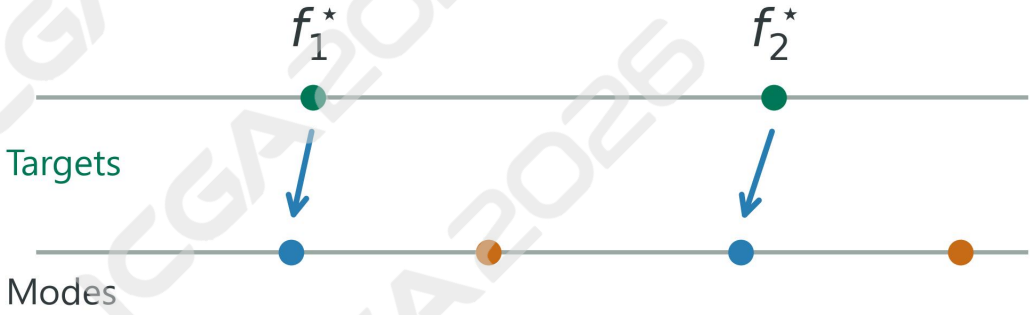
$$\min_{\boldsymbol{s}} \; J_{\text{multi}} = \lambda_0 \mathcal{P}_a + \lambda_1 \mathcal{P}_r$$

$$\text{subject to} \quad \frac{V(\boldsymbol{s})}{V_D} \le \overline{V}.$$

λ_0 and λ_1 balance attraction and repulsion.

Why can't the single-target selection method continue to be used?

With several targets, the same mode may be selected more than once.



One-to-one assignment matches each target to a different mode.

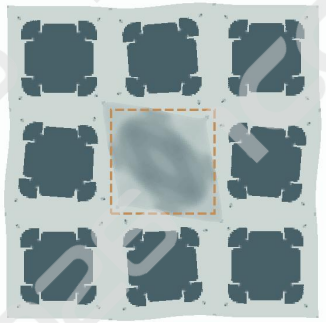
Target Placement and Mode Separation

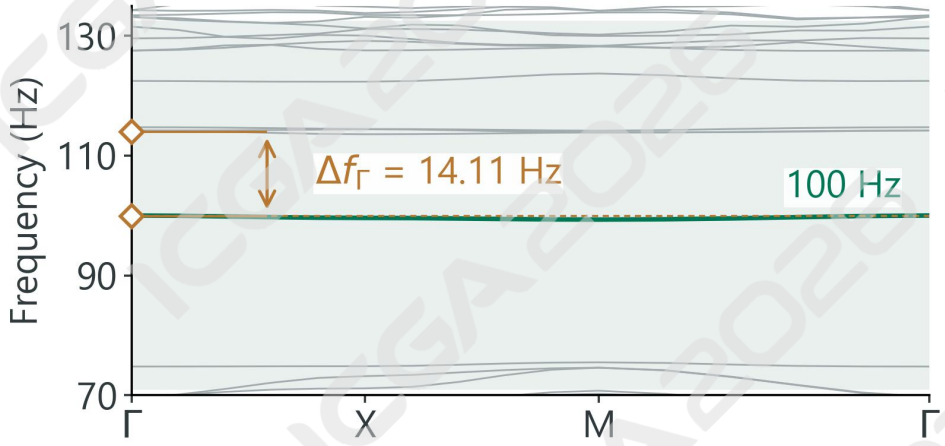
Matching the target frequency alone does not control neighboring defect modes.

$$J_{\text{single}} = \underbrace{\sum_{j\in\mathcal{D}} S_j P_a(f_j)}_{\text{Attraction}} + \underbrace{w_r \sum_{j\in\mathcal{D}} (1-S_j) P_r(f_j)}_{\text{Repulsion}}$$

Attraction only

Match the target frequency.



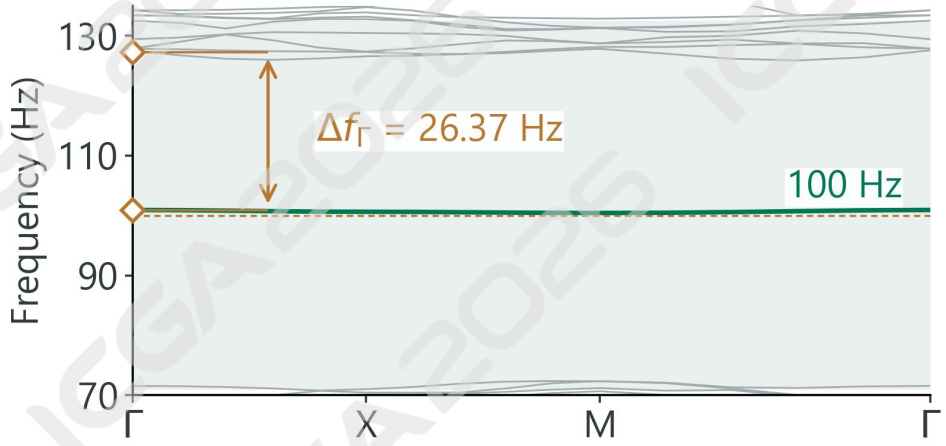


Attraction + Repulsion

Match the target frequency.

Move competing modes outward.



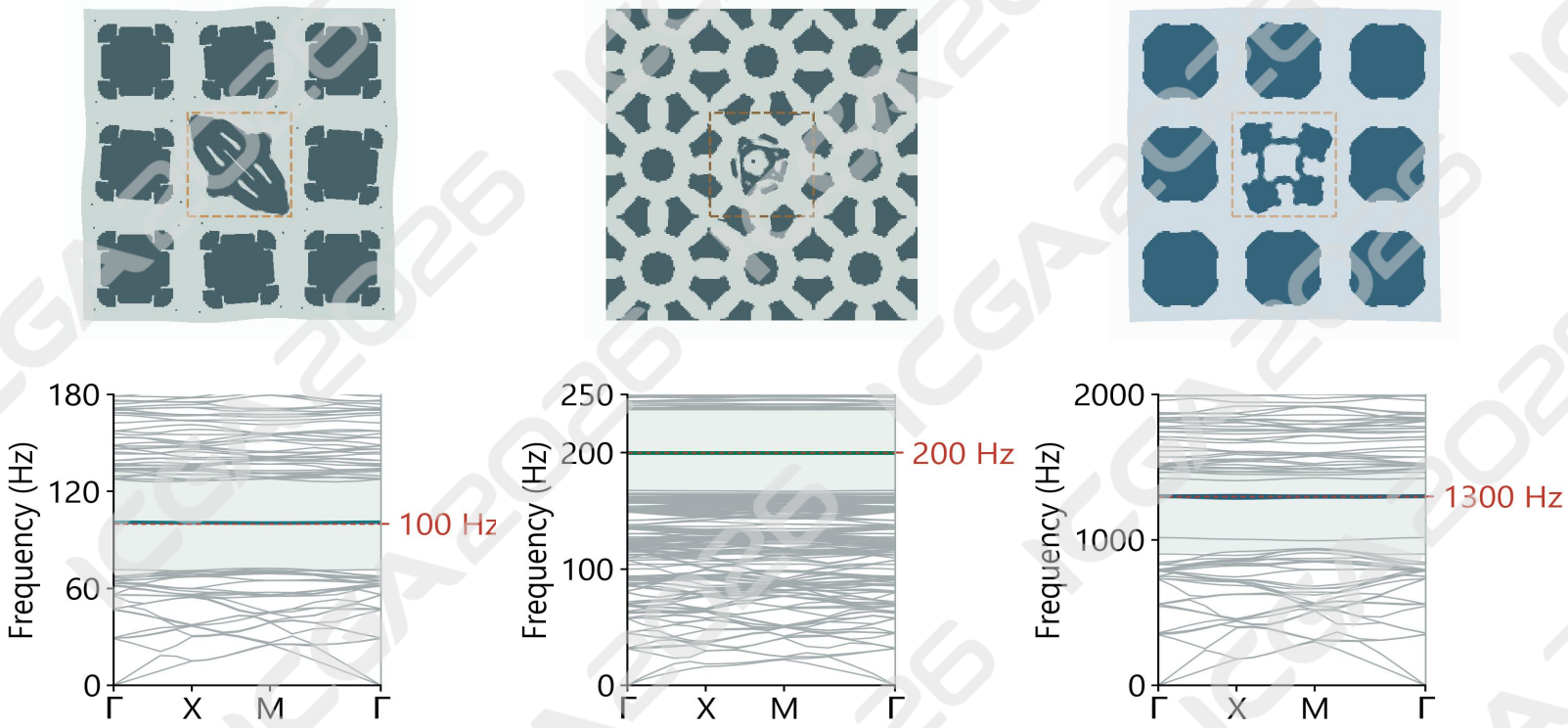


Nearest-mode separation increases from 14.11 to 26.37 Hz (+87%).

Model Reduction for Defect Optimization

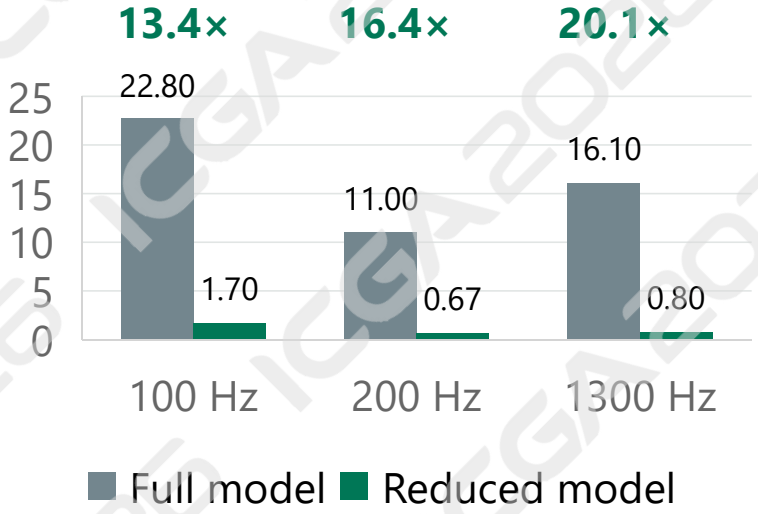
NAGOYA UNIVERSITY

100 Hz **200 Hz** **1300 Hz**



Same design in each structure–dispersion pair.
The 1300 Hz case uses a different material contrast.

Stage II optimization time (h)



Property	100 / 200 Hz	1300 Hz
E_1 / E_2 (GPa)	0.02 / 0.50	3 / 70
ρ_1 / ρ_2 (kg/m³)	1000 / 3000	1180 / 2700
ν_1 / ν_2	0.30 / 0.30	0.35 / 0.35

CB reduction reuses the fixed host and updates only the central defect.

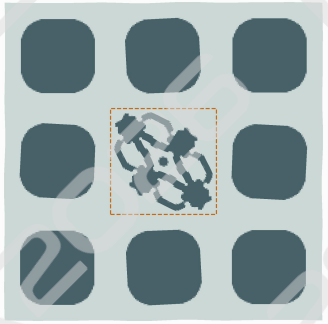
Localized modes at two target frequencies

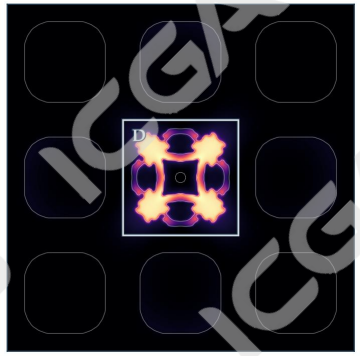
One optimized defect supports localized modes near 9000 Hz and 14000 Hz.

Material	E (GPa)	ρ (kg/m^3)	ν
1	4.35	1180	0.37
2	210.0	7780	0.30

Mode shape **Kinetic energy**

9000 Hz target

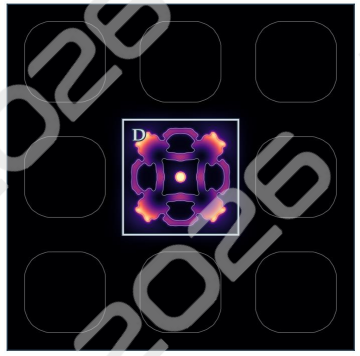




84.3% in the defect

14000 Hz target

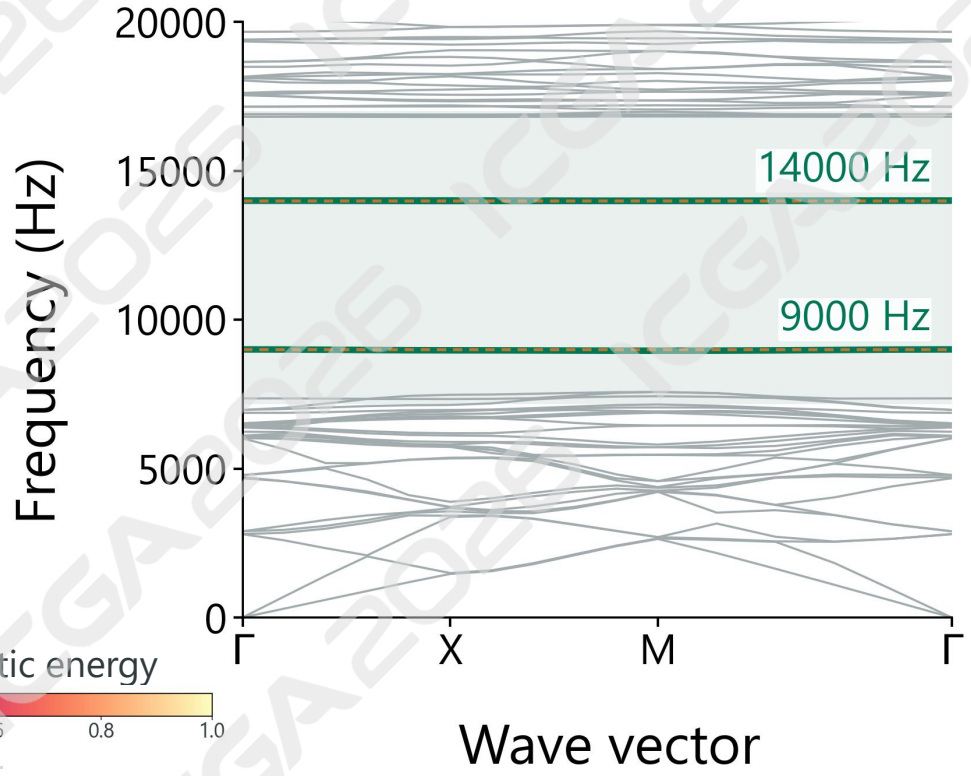




91.0% in the defect



Host gap and defect modes

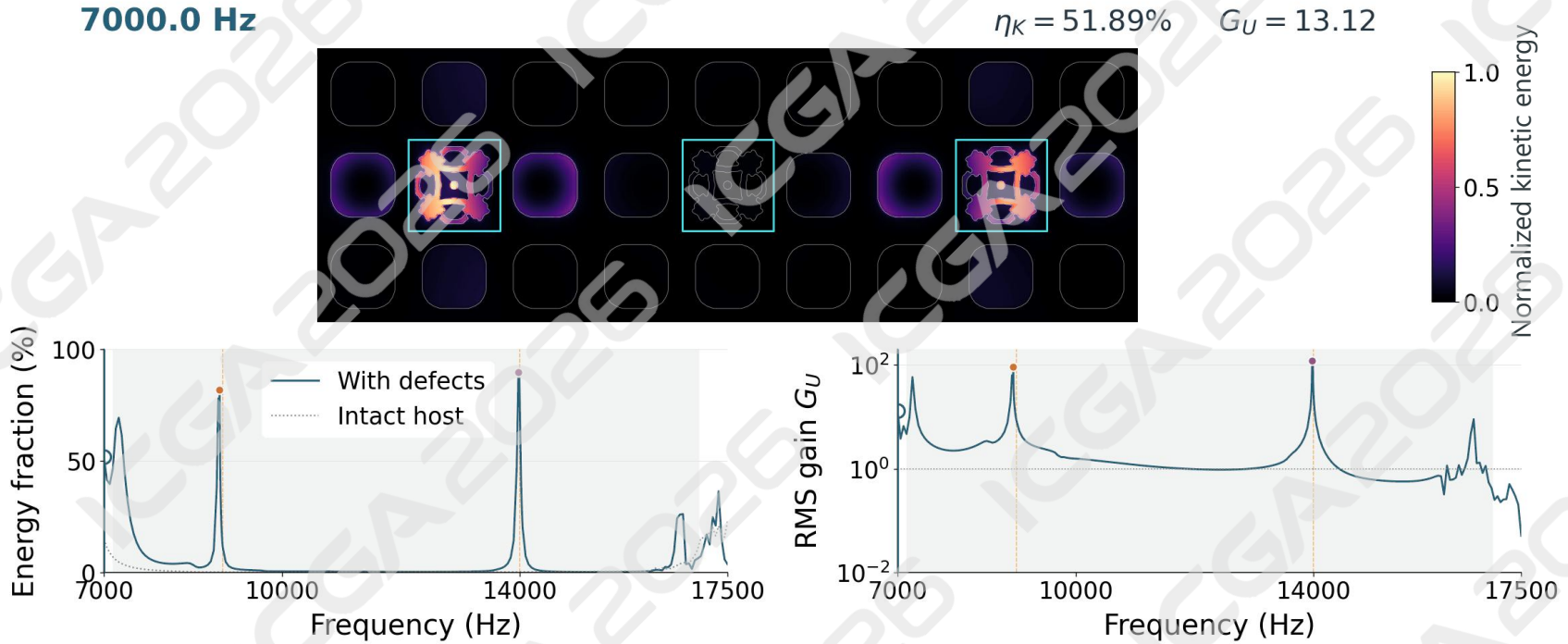


Different localized mode shapes coexist in the same defect.

Verification | vibration localization

Why validate?

Check whether localization persists under an applied load in a finite sample.



Energy concentration

Fraction of sample kinetic energy in the three defect cells.

Local amplification

Defect-region RMS displacement relative to the intact host.

How to read the sweep

The frequency marker and energy field advance together.

Colors show the energy patern.

Compare concentration and amplification to identify localized resonant responses.

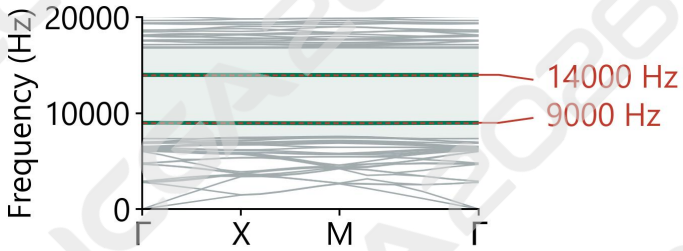
Multiple Resonances in one defect

Target frequencies and localized modes

Corresponding dispersion

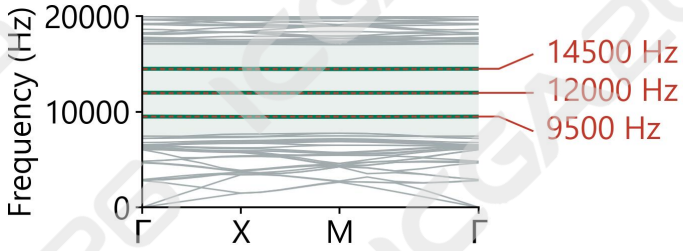
2 targets



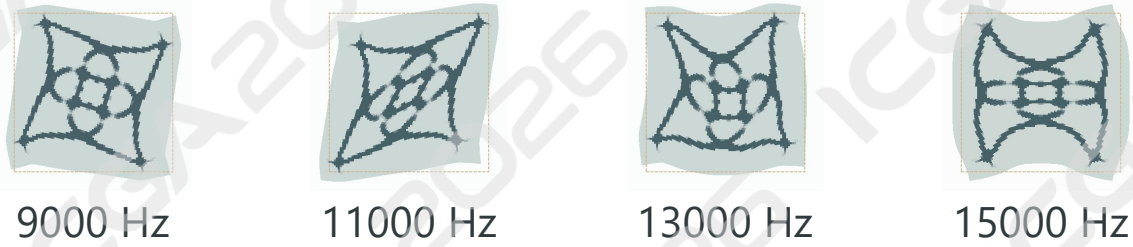


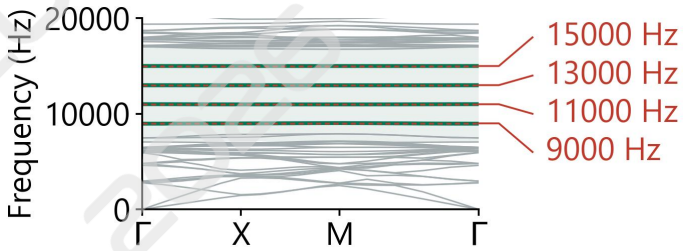
3 targets





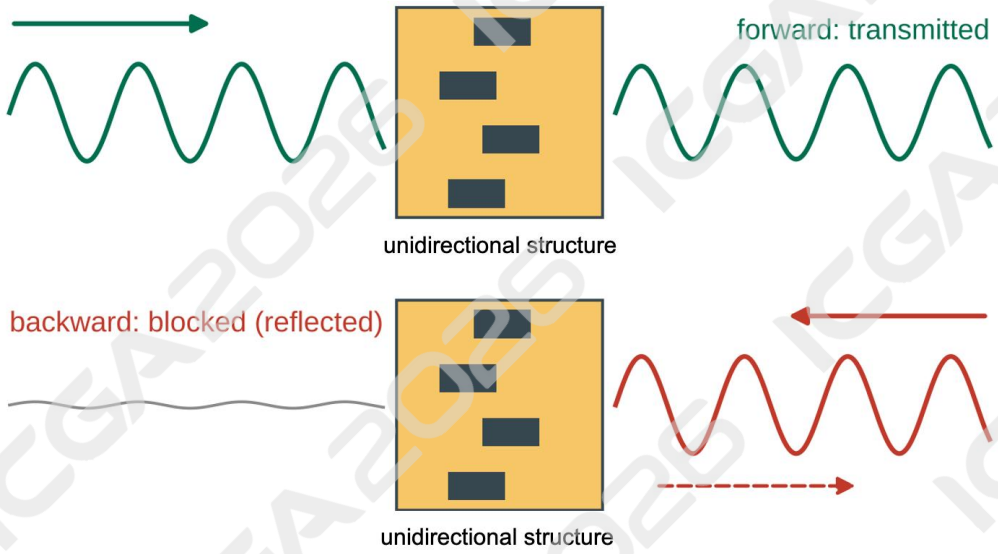
4 targets





Two to four prescribed frequencies can be accommodated in one defect.

Asymmetric elastic-wave transmission

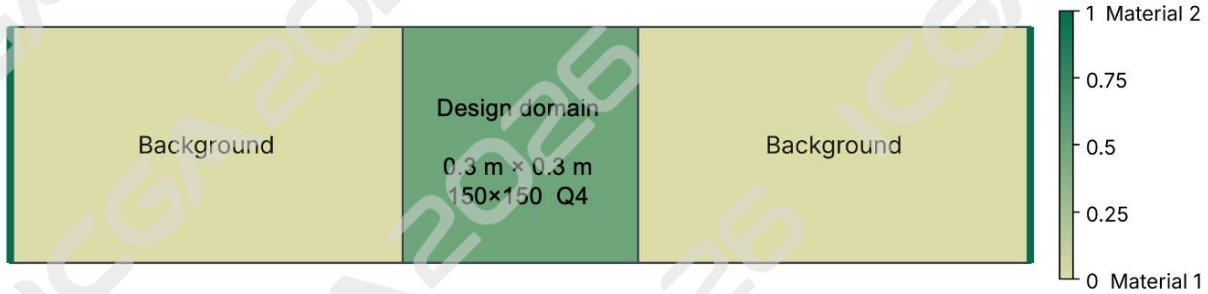


$$\underset{\bar{s}}{\text{minimize}} \quad f(\bar{s}) = \frac{1}{N_f}\sum_{k=1}^{N_f}\left[T_{R\to L}(\omega_k) - T_{L\to R}(\omega_k)\right]$$

$$\text{subject to} \quad g_V(\bar{s}) = \frac{V(\bar{s})}{V_{\text{lim}}} - 1 \le 0,$$

$$g_G(\bar{s}) = \frac{G(\bar{s})}{G_{\text{lim}}} - 1 \le 0,$$

$$0.0 \le \bar{s} \le 1.0.$$



Applications: Unidirectional wave transmission enables vibration isolation, noise shielding, directional energy harvesting and signal routing.

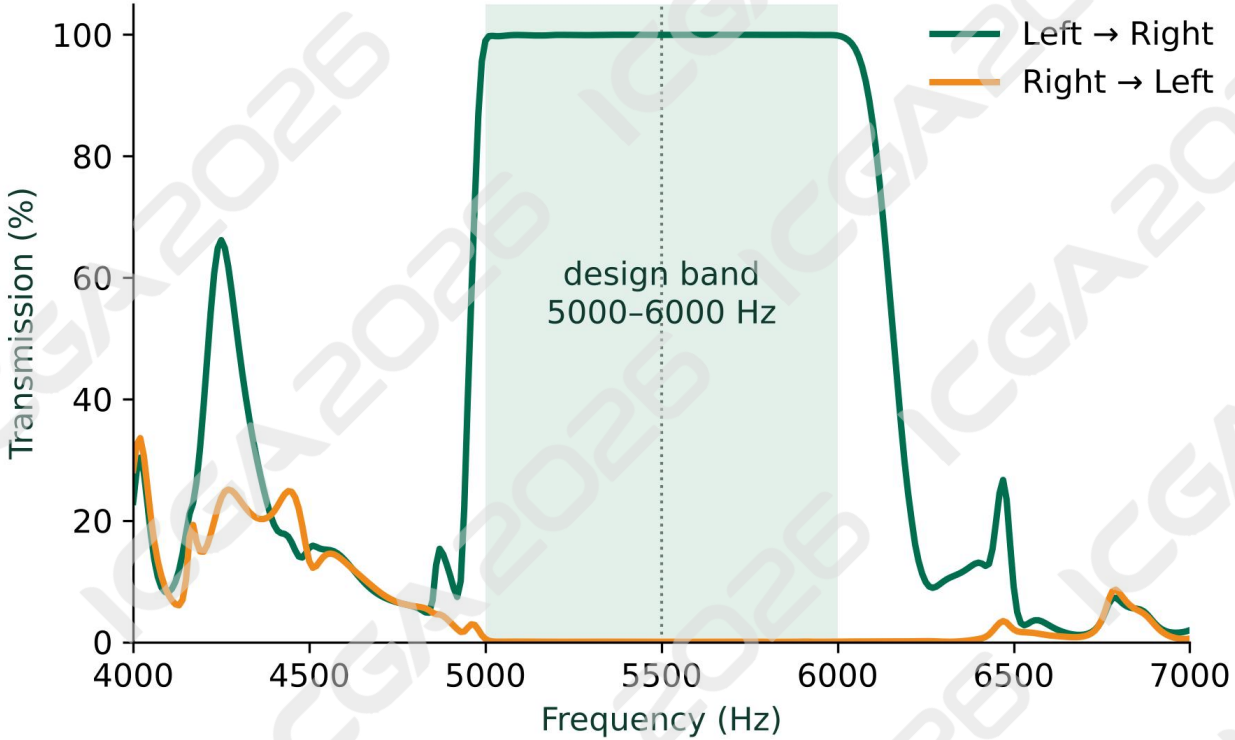
Mechanism: A topology-optimized structure converts an incident P-wave into an S-wave in one direction and reflects it in the other.

- **Left / Right boundaries:** exact modal DtN ports
- **Top / Bottom:** periodic

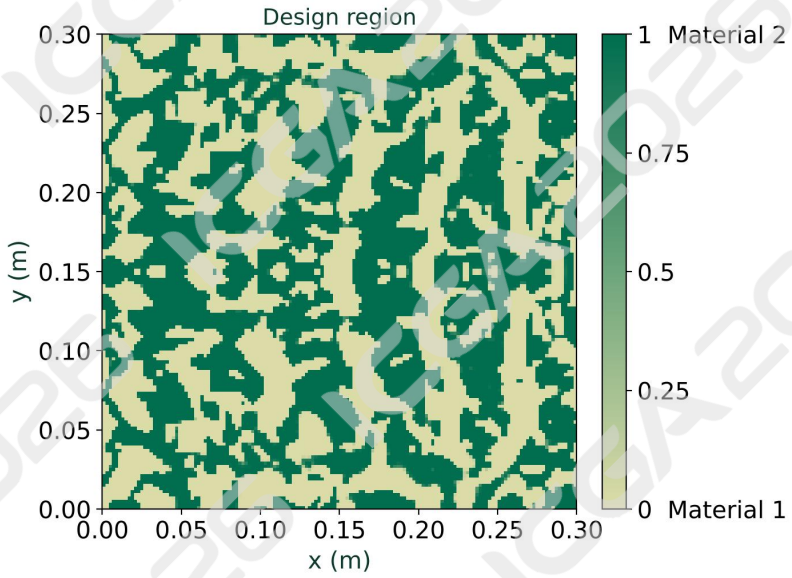
Material	E(Pa)	P(kg/m³)	ν
1	5×10^8	2000	0.3
2	5×10^9	8000	0.3

NAGOYA UNIVERSITY

Asymmetric elastic-wave transmission



Transmission versus frequency



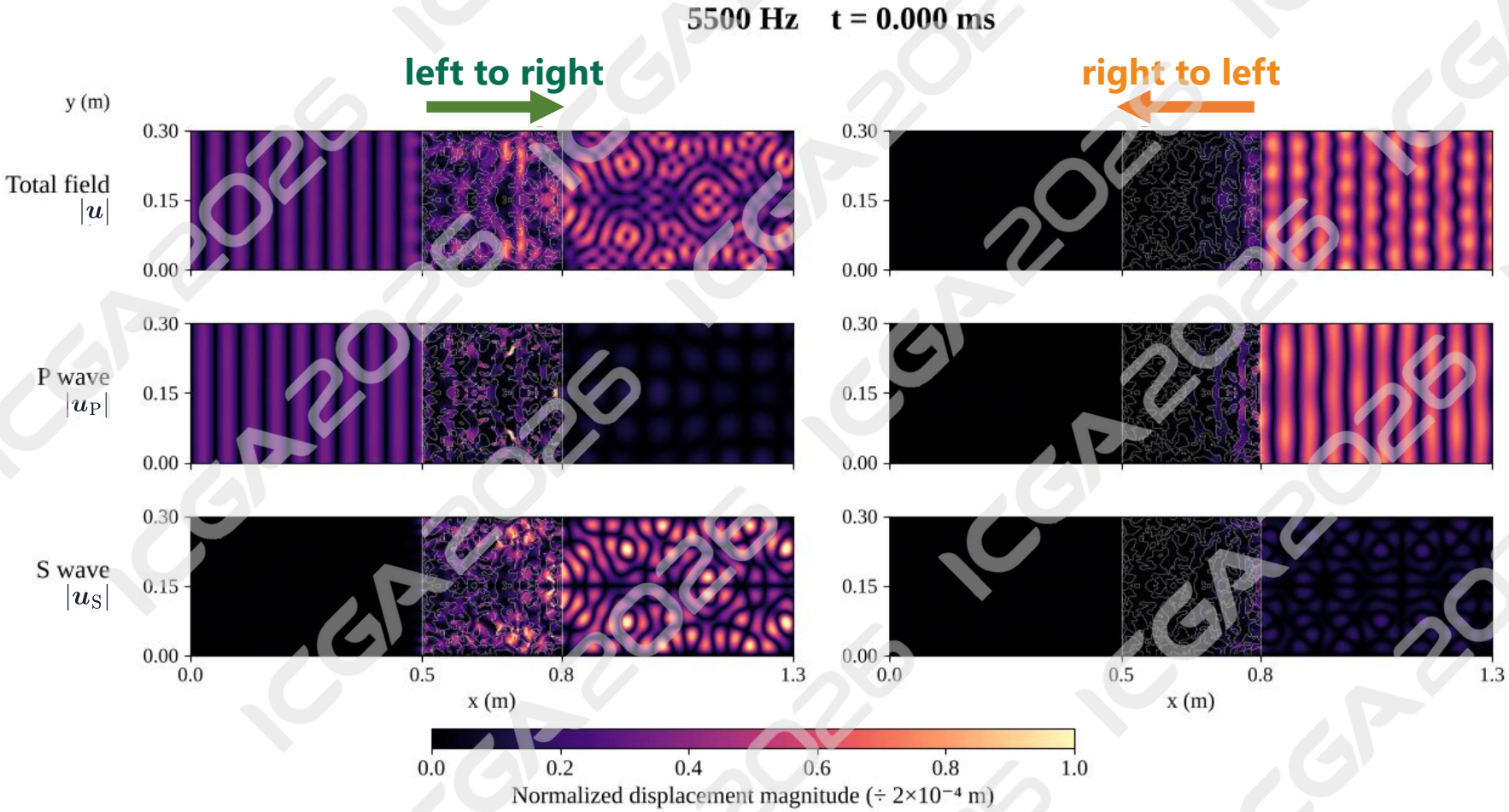
designed metamaterial

Shaded band is the design band 5000–6000 Hz.

Inside the band

- Forward transmission averages 99.93% (minimum 98.98%)
- Backward transmission averages 0.04% (maximum 0.49%)

Asymmetric elastic-wave transmission



left to right

99.97% of the energy is transmitted

right to left

0.02% of the energy is transmitted

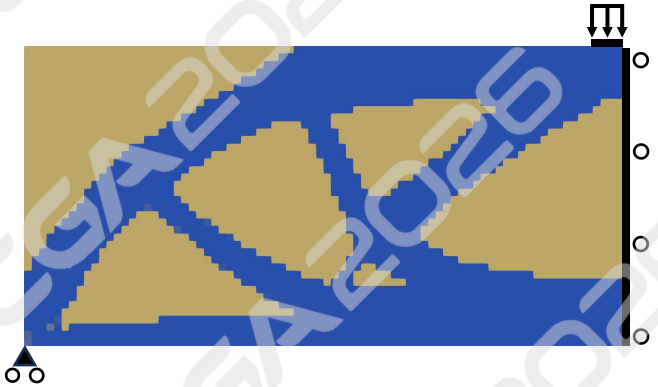
Left-to-right: the P-wave is converted into an S-wave inside the structure (77% S, 23% P)

Right-to-left: it is reflected (98%) and builds a standing wave on the right, leaving the left side almost at rest.

Conclusions and future perspectives

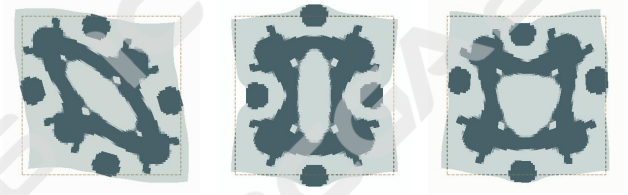
Nonlinear multi-material TO

- Stabilized ductile and quasi-brittle TO by smoothing functions
- Updated Adjoint-Free SA (ANSA) and achieved low computational cost
- Stress interpolation avoided complicated SA derivation and grayscale

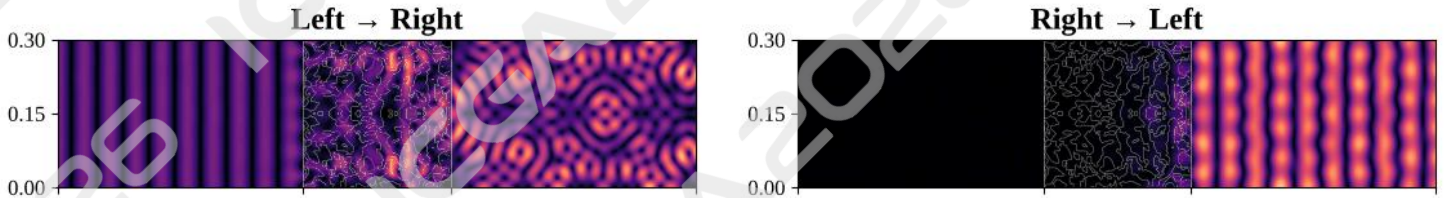


Vibration / Wave metamaterial design

- Bandgap & selective defect mode control / Frequency-selective transmission
- Direction-dependent wave control & Metamaterial design



9500 Hz 12000 Hz 14500 Hz



Prospects

- **Toward next-generation metamaterials** by integrating nonlinear multi-material phenomena and wave control

Selected Publications

Selected journal papers

2026 **Xu, Nishiguchi & Kato**
A two-stage topology optimization framework for designing multi-scale elastic metamaterials with cross-scale dual bandgaps
CMAME

2026 **Nara & Kato**
Multi-material topology optimization of ductile and quasi-brittle materials with gradient-continuous constitutive law
CMAME

2026 **Liu et al.**
Multi-material dynamic topology optimization of reaction force minimization problem with viscoelasticity
Finite Elements in Analysis and Design

2026 **Nakano, Nishiguchi & Kato**
A QUBO Formulation for Multi-Material Topology Optimization With Quantum Annealing
IJNME

2026 **Takaara, Nishiguchi & Kato**
Topology optimization of microstructures considering multi-scale thermo-fluid problems
SMO

2025 **Xu et al.**
Variable Density Interpolation for Dynamic Topology Optimization
IJNME

2025 **Nara et al.**
Stability-enhanced topology optimization applying a subloading surface penalty to elastoplastic materials
SMO

FACULTY PROFILE
Nagoya University (EN)

LAB WEBSITE
www.nuopt.org

2025 **Matsui et al.**
Multiscale Topology Optimization Applying FFT-Based Homogenization
IJNME

2025 **Katsumata et al.**
Topology Optimization for Large-Scale Unsteady Flow With the Building-Cube Method
IJNME

2018 **Kato, Yachi, Kyoya & Terada**
Micro-macro concurrent topology optimization for nonlinear solids with a decoupling multiscale analysis
IJNME 113(8), 1189–1213 | DOI: 10.1002/nme.5571

2015 **Kato, Hoshiba, Takase et al.**
Analytical sensitivity in topology optimization for elastoplastic composites
SMO 52(3), 507–526 | DOI: 10.1007/s00158-015-1246-8